**Aalborg Universitet**

AALBORG UNIVERSITY

# A comparative study on three reactor types for methanol synthesis from syngas and CO2

Cui, Xiaoti; Kær, Søren Knudsen

*Published in:*
Chemical Engineering Journal

*DOI (link to publication from Publisher):*
10.1016/j.cej.2020.124632

*Creative Commons License*
CC BY-NC-ND 4.0

*Publication date:*
2020

*Document Version*
Accepted author manuscript, peer reviewed version

Link to publication from Aalborg University

*Citation for published version (APA):*
Cui, X., & Kær, S. K. (2020). A comparative study on three reactor types for methanol synthesis from syngas and CO2. *Chemical Engineering Journal*, *393*, Article 124632. https://doi.org/10.1016/j.cej.2020.124632

**General rights**
Copyright and moral rights for the publications made accessible in the public portal are retained by the authors and/or other copyright owners and it is a condition of accessing publications that users recognise and abide by the legal requirements associated with these rights.

- Users may download and print one copy of any publication from the public portal for the purpose of private study or research.
- You may not further distribute the material or use it for any profit-making activity or commercial gain
- You may freely distribute the URL identifying the publication in the public portal -

**Take down policy**
If you believe that this document breaches copyright please contact us at vbn@aub.aau.dk providing details, and we will remove access to the work immediately and investigate your claim.

Downloaded from vbn.aau.dk on: December 05, 2025

# A comparative study on three reactor types for methanol synthesis from syngas and $CO_2$

Xiaoti Cui, Søren Knudsen Kær

*Department of Energy Technology, Aalborg University, Pontoppidanstr. 111, 9220 Aalborg øst, Denmark*

**Abstract**

In this study, a comparative study was conducted on the three reactor types (the adiabatic, water-cooled and gas-cooled reactor) employed for the traditional syngas to methanol (STM) process to investigate their potential applications to the STM process with the $CO_2$-rich feed gas or the $CO_2$ hydrogenation to methanol (CTM) process. The temperature profiles in the axial and radial directions particularly the hot-spot temperatures, operating conditions and methanol yields for the reactors have been investigated using the thermodynamic analysis, the CFD method and the pseudo-homogeneous model. The capital costs for CTM process with the three reactor types have also been evaluated. Compared with the traditional STM process, the STM process with the $CO_2$–rich feed gas and CTM process exhibited reduced hot-spot temperatures. The simulation results showed that the single-bed adiabatic (without internal cooling) reactor and the gas-cooled reactor exhibited potentials for the CTM process, where the hot-spot temperatures the hot-spot temperatures in the reactors can be within the typical operating temperature range (e.g., 220–280 °C) for the catalyst. Regarding the comparison of the three reactor types for the CTM process, the water-cooled

reactor showed advantages in terms of efficient heat removal, low hot-spot temperature and wide relatively range inlet temperature for control. The adiabatic reactor and the gas-cooled reactor demonstrated a relatively low and medium performance, and also a relatively low and medium capital cost, respectively, which indicates the potentials of the two reactor types in a small-scale CTM process.
*Keywords:* Methanol synthesis, $CO_2$ hydrogenation to methanol, Thermodynamic analysis, Adiabatic reactor, Water-cooled reactor, Gas-cooled reactor

## 1. Introduction

The hydrogenative chemical recycling of $CO_2$ from natural or industrial sources has attracted significant attention in recent years as a possible route to reducing $CO_2$ emissions, where $H_2$ can be produced by water electrolysis with renewable energy sources [1, 2]. Particularly, it is a crucial step for the concept of the "methanol economy" where methanol can be used as fuel and a raw material for the products conventionally derived from fossil fuels [3]. Nowadays, the route via $CO_2$ hydrogenation to methanol (CTM) is being discussed globally in the aspects of technology and economy [4, 5, 6, 7, 8, 9, 10, 11].

From the technology point of view, the CTM process is considered in technology readiness levels (TRLs) 6–7 [8], which are developed based on the mature technology of the syngas (CO is the main carbon source) to methanol (STM) process using gas-phase catalytic fixed-bed reactors. Conversely, other potential methods, e.g., electrochemical and photochemical

methods [12, 13], the membrane reactor [14], and the slurry phase reactor [15], are at the research stage. The traditional CTM process is typically operated at pressures of 50–100 bar and temperatures of 200–300 °C, and it involves the hydrogenation of CO and $CO_2$ and reverse watergas shift (RWGS) reactions:

$$\mathrm{CO} + 2\,\mathrm{H_2} \longleftrightarrow \mathrm{CH_3OH} \qquad \Delta H_{298\mathrm{K}} = -91\,\mathrm{kJ/mol} \tag{1}$$

$$\mathrm{CO_2} + 3\,\mathrm{H_2} \longleftrightarrow \mathrm{CH_3OH} + \mathrm{H_2O} \qquad \Delta H_{298\mathrm{K}} = -49\,\mathrm{kJ/mol} \tag{2}$$

$$\mathrm{CO_2} + \mathrm{H_2} \longleftrightarrow \mathrm{CO} + \mathrm{H_2O} \qquad \Delta H_{298\mathrm{K}} = 41\,\mathrm{kJ/mol} \tag{3}$$

Compared with the conventional exothermic STM process, the CTM process generates less reaction heat from the reaction (2), and the endothermic side-reaction (3) can weaken the heat release of the process. Additionally, water is formed as a by-product in the CTM process which has a detrimental effect on the conventional copper-based catalyst and results in the deactivation of the catalyst [16]. The problem can be addressed through a two-step process, including the RWGS process and methanol synthesis process. Moreover, the by-product (water) formed in the RWGS process can be removed before the latter process, which is also referred to as the CAMERE process (carbon dioxide hydrogenation to methanol via reverse water–gas shift) [17]. Additionally, the applications of novel membrane reactors and sorption-enhanced reaction processes can be a potential method for removing the by-product (water) for a one-step CTM or CAMERE process [18, 19, 20, 21], which is at the laboratory level. Compared with the CAMERE process, the one-step CTM process has a less complex system and only requires the methanol synthesis component (typically requires one or

two methanol synthesis reactors). The present study focused on the reactor designs for the one-step CTM process (hereinafter referred to as the CTM process). Nowadays, the performance of modern catalysts is being improved, which could also increase the feasibility of the application of the CTM process, e.g., a stability pilot-scale test of 700 h was carried out for the CTM process using the commercial Süd-Chemie (now Clariant) catalyst in Ref. [4]. The catalyst exhibited good activity and selectivity, and a deactivation rate similar to that for the STM process. Bukhtiyarova et al. [22] conducted a large laboratory-scale test using the $Cu/ZnO/Al_2O_3$ catalyst for the CTM process. The results of the stability test (up to 325 h) also showed a similar deactivation rate to that reported for the STM process. Additionally, many studies have focused on the catalyst development for the CTM process on the research level [23, 24, 25, 26, 27]. The conventional methanol reactors for the STM process can be used for the CTM process with proper modifications. The traditional STM process has been employed for nearly a hundred years [28]. Many types of commercial reactors have been developed, which are reviewed in the Ref. [29, 30, 31]. The main issues regarding the reactor design include the removal of the reaction heat, pressure drop, cost, and scalability [29]. The reactors can be divided into two main types according to the method of heat removal in the catalyst beds: 1) adiabatic reactor ; 2) isothermal (or internal cooling) reactors [28]. The first type has comparatively simple structures with one or more adiabatic catalyst beds. For a typical adiabatic reactor with multiple catalyst beds, gas quenching is usually employed to lower the gas temperature after each bed, e.g., the ARC (advanced reactor concept) quench-cooled converter from Casale [30].

The second type integrates tubes or plates for heat removal from the catalyst beds, which results in more complex reactor structures and increased capital cost. However, this type of reactor provides a highly efficient heat transfer process and a more uniform temperature distribution in the reactor; for instance, the Lurgi (now Air Liquide) methanol reactor is widely used in the industry. It has a shell-tube structure, and the boiling water provided in the shell side can efficiently remove the reaction heat released in the tube side with the catalyst loaded. Additionally, a gas-cooled (or tube-cooled) reactor may be added in the condition where a relatively large production capacity is required, such as the two-step Lurgi's mega-methanol process. With respect to the reactor modeling for the CTM process, the selection of the reaction types and designs under different conditions (e.g., reactor scale, capital cost and available utilities) for both the STM and CTM processes can be evaluated by modeling studies which have been thoroughly reviewed by Bozzano and Manenti [30] in the aspects of reaction kinetics, mass transport limitations, catalyst deactivation, steady-state, and dynamic models. Meyer et al. [32] conducted a two-dimensional pseudo-homogeneous reactor modeling study for the CTM process, and compared the two commonly used kinetic models (by Graaf et al. [33] and Bussche and Froment [34]). The results showed differences in the first half of the reactor using the two kinetic models, which also indicated that attentions should be paid to the selection of kinetic models for the CTM process. Samimi et al. [35] investigated the possibility of liquid formation in the reactors at an industrial scale CTM process at high pressures (50–300 bar). The water-cooled, gas-cooled and double-cooled (cooled by both water and gas) reactor types were compared

in the modeling studies, and the gas-cooled reactor showed a lower possibility of liquid formation and better $CO_2$ conversion and methanol yield than the others. Marlin et al., [10] from Carbon Recycling International (CRI), discussed the main difference in the reactor design and distillation system between the CTM and STM processes. Tube-cooled (or gas-cooled) reactors were recommended which are more efficient than adiabatic reactors and simpler than water-cooled reactors. Leonzio et al. [36] presented pseudo-homogeneous reactor modeling studies on the adiabatic and water-cooled reactor for the CTM process; acceptable temperatures <280 °C were obtained for the adiabatic reactor, and sensitive analysis of the global heat transfer coefficient (300–1000 $W/(m^2 \cdot K)$) were investigated for the water-cooled reactor. However, the reported modeling study regarding the reactor designs for the CTM process at an industrial scale, or for the reactor modifications or considerations required when changing from the STM to the CTM process are still limited, moreover, the application of different reactor types to the CTM process is rarely discussed. In the present study, the application of three commonly used reactor types (adiabatic, water-cooled and gas-cooled) to the CTM process were investigated by comparing with the conditions and reactor designs for the traditional STM process. The main issues associated with the thermodynamic analysis for the adiabatic reactor, radial heat transfer for the water-cooled reactor and hot-spots for the three reactor types were addressed. The performance comparison with the key performance indicators (KPI) was also conducted among the three reactor types to investigate their potentials in application to the CTM process or STM process with $CO_2$-rich feed gas.

## 2. Modeling approach

### *2.1. Thermodynamic analysis*

Thermodynamic analysis can provide quick evaluations for the streams in the CTM process, such as the possible composition and temperature, after the reaction in the methanol reactor. In this study, the Gibbs free energy minimization method is used to predict the thermodynamic equilibrium. For the gas-phase reaction system in the CTM process using the Lagrange multiplier method, the Gibbs free energy minimization for the system can be expressed by the following equations considering each species in the gas phase and the total system [37]:

$$\triangle G_{fi}^{0g} + RTln\frac{y_i\phi_i P}{p^0} + \sum_k a_{ik}\lambda_k = 0 \tag{4}$$

$$\sum_{i=1}^{N} n_i(\triangle G_{fi}^{0g} + RTln\frac{y_i\phi_i P}{p^0} + \sum_k a_{ik}\lambda_k) = 0 \tag{5}$$

with the following constraint:

$$\sum_i n_i a_{ik} = A_k \tag{6}$$

where $\triangle G_{fi}^{0g}$ is the standard Gibbs free energy for the formation of gaseous species i; $y_i$ is the mole fraction of species i; $P$ and $P^0$ are the system pressure and standard state pressure (1 atm), respectively; $\phi_i$ is the fugacity coefficient of species i; $n_i$ is the mole number of species i; $\lambda_k$ is the Lagrange multiplier; $a_{ik}$ is the number of atoms of the $k^{th}$ element in each molecule of gaseous species i, and $A_k$ is the total atomic mass of the $k^{th}$ element in the feed.

The thermodynamic studies for the CTM process under isothermal have been reported in the literature [38, 39, 40, 41, 42]. With respect to the adiabatic conditions, the influence of the CO and $CO_2$ content (SN>2) in the feed gas have been investigated at a certain operating condition of P= 5 MPa and $T_{in}$= 200 °C[43], however, calculations for the adiabatic condition with wide ranges of temperature and pressure are still required for the reactor designs. In the present study, the conventional feed gas conditions (in methanol industry) of $T_{in}$= 180–280 °C, P= 30–80 bar, SN= ($H_2$ mol–$CO_2$ mol)/(CO mol+$CO_2$ mol)= 2–10 and CO mol/(CO mol+$CO_2$ mol)= 0–1 were considered for the CTM and STM processes under the adiabatic condition (Section 3.1), where SN value represents the relative H2 content comparing with those of the CO and CO2 in the feed gas, the stoichometries of reaction 2 and 3 were fufilled when SN=2. Notably, the $T_{in}$ value lower than 180 °C and higher than 280 °C were not considered, which may increase the risk of wax condensation in the catalyst bed and catalyst deactivation by sintering, respectively. A flow rate of 1.0 kmol/s was set for $CO_x$ ($CO_x$ denotes the sum flow rate of CO and $CO_2$) in the feed stream. The calculation was conducted using the Aspen Plus software. The Gibbs reactor was used with the same pressure as that of the feed stream and zero heat duty. The predictive Soave-Redlich-Kwong (PSRK) model was used as the equation of state. The adiabatic CTM process includes both the single-pass process and the process with the recycle stream (shown in Fig. 1). The main components in the system are $H_2, H_2O, CO, CO_2$, and methanol. Other possible byproducts for the methanol synthesis process such as DME, alcohols, and paraffin were not considered.

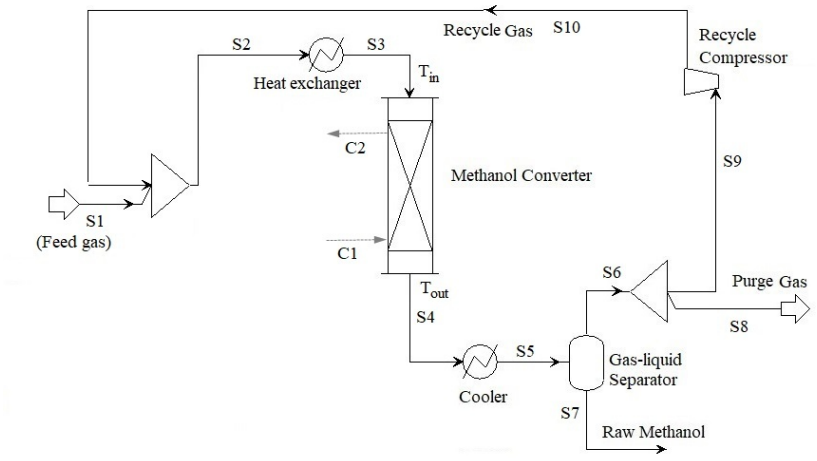


(a)

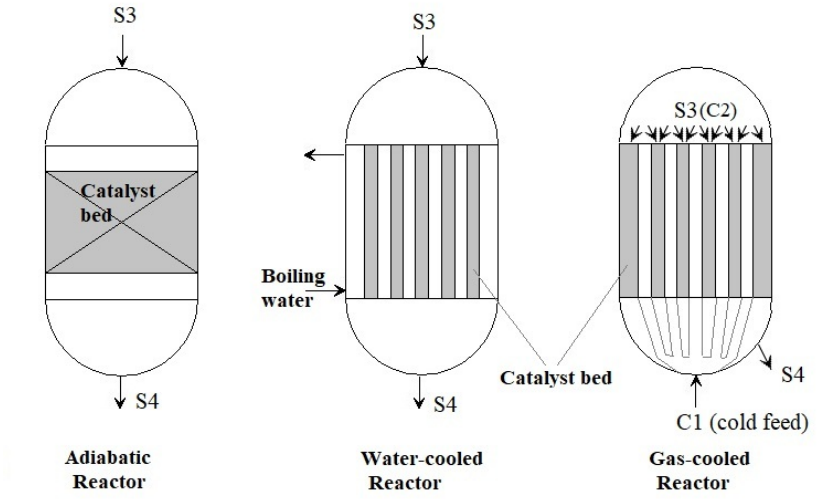


(b)

Figure 1: (a) Scheme of the CTM or STM process and (b) methanol converters.

*2.2. Pseudo-homogeneous model*

The one-dimensional pseudo-homogeneous model is commonly used for the conventional STM process in a packed bed reactor, where negligible gradients are assumed between the gas and solid phases [30]. Other assumptions also include the negligible radial and axial diffusion and uniform velocity, temperature and pressure in the radial direction [30], which are reasonable for an industrial-scale methanol reactor usually with long reactor tubes (e.g., 7 m) and a small tube diameter (e.g., 40 mm). In this study, the pseudo-homogeneous plug-flow reactor in the ASPEN software was used to describe the STM and CTM processes in Sections 3.2–3.4. The reaction kinetics proposed by Bussche and Froment [34] was used to evaluate the reaction rates under different conditions (parameters shown in Appendix A), which assumed only the route of $CO_2$ hydrogenation to methanol (reaction (2)) and the RWGS reaction (reaction (3)). An average effectiveness factor for the catalyst bed was used, which was evaluatd by the CFD modeling in the following section. The heat transfer between the gas phase in the packed-bed and the boiling water (Section 3.2) or cold feed (Section 3.3) were evaluated by the correlations for heat transfer coefficients in the literature [44, 45, 46, 47] (Appendix C). A typical catalyst tablet of $\Phi 6 \times 4$mm (e.g., Topsøe MK-121) was used, and the pressure drop of the catalyst bed was evaluated by the Ergun equation[32](Appendix A). The tube diameter and length for the water-cooled or gas-cooled reactor were set to 40 mm and 3 m, respectively; a larger tube diameter of 100 mm was only considered in Section 3.2. Various tube numbers were used to achieve a gas hourly space velocity (GHSV) close to the typical industrial value of 10000 $h^{-1}$ for each

case. A total flow rate of 16 kmol/h was set for the $CO_x$ in the feed stream, while the flow rate of $H_2$ was set according to SN= 2. The flow rate settings resulted in a methanol production of around 4000 ton /year, which is the same as the production capacity of the renewable methanol plant in Iceland [10]. The conditions with the recycle stream was considered where 99.9% of the unconverted gas (stream S9 in Figure 1(a)) was recycled. The single-pass methanol yield or local methanol yield in the reactor is given by

$$y_{MeOH} = \frac{n_{MeOH,S4(orL)} - n_{MeOH,S3}}{n_{CO_2,S3} + n_{CO,S3}} \tag{7}$$

where S3 and S4 are the streams at the inlet and outlet of the catalyst bed (show in Fig. 1), respectively, and $L$ represents a local position along the catalyst bed.

### *2.3. CFD models*

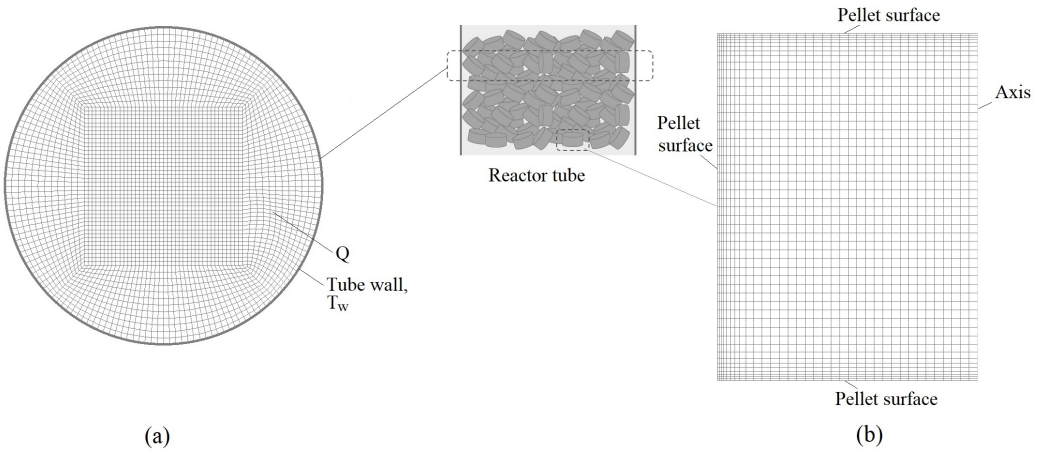


Figure 2: Scheme of (a) the tube cross-section and (b) catalyst tablet for the 2-D CFD model.

With respect to the comparisons of the radial heat transfer in the reactor tube under different conditions, a simple two-dimensional CFD model was used as shown in Figure 2(a). The radial heat transfers at certain cross-sections (hot-spots) of the reactor tube were considered and described by pseudo-heat conduction with an effective conductivity ($k_{e,r}$) (Appendix C), which is usually used to estimate the radial heat transfer for a packed bed or monolith reactor [48]. The operating conditions of pressure and gas composition at the hot spots (A–F in Figure 6) were uniformly distributed in the cross-section. The influence of the near-wall region was also considered by a heat transfer coefficient ($h_w$) (Appendix C), which may result in a temperature jump near the wall. The heat conduction in the wall was also included with a typical thickness of 2 mm and thermal conductivity of 18 W/m $\cdot$ K [49]. The temperature of $T_w$= 250 °C and relevant temperature of the cold feed gas were set for the boiling water reactor and gas-cooled reactor, respectively. The tube radius (inner radius) of R= 20–50 mm was considered to investigate the influence of the tube size. The steady state energy equation for the heat conduction is expressed by

$$\nabla \cdot (k_{e,r} \nabla T) + Q = 0 \tag{8}$$

where the source term Q (W/m$^3$) is the reaction heat based on the bulk volume of the catalyst bed and is calculated by

$$Q = -\rho_{cat}(r_{MeOH} \triangle H_{MeOH} + r_{RWGS} \triangle H_{RWGS}) \tag{9}$$

where $r_{MeOH}$ and $r_{RWGS}$ are the reaction rates (kmol/kg$_{\mathrm{cat}}$·s) for reaction (2) and (3), and $\triangle H_{MeOH}$ and $\triangle H_{RWGS}$ are the reaction enthalpies (J/kmol)

for reaction (2) and (3), respectively; $\rho_{cat}$ is the bulk density of the catalyst bed (1300 kg/m$^3$) or the density of the catalyst tablet (1950 kg/m$^3$) for the two models in Figure 2; $r_{MeOH}$ and $r_{RWGS}$ were calculated by the user defined functions based on the reaction kinetics (Appendix A), and the reaction enthalpies at different temperatures are approximated by Aspen Properties (Appendix A). The simulations were conducted using the commercial finite-volume-based solver ANSYS FLUENT 19.0, in the parameter optimization studies with double precision.

Additionally, a single catalyst tablet ($\Phi$6×4mm) was modeled for investigating the effectiveness factor of the catalyst tablet under different conditions, and a 2-D axisymmetric geometry was employed as shown in Figure 2(b). Stuidies on the evaluations of the effectiveness factor were reported in the literatures using modified Thiele modulus [50, 30, 51]. In the present study, the effectiveness factor was evaluated by the 2-D CFD model. The heat conductivity in the catalyst tablet was considered with similar expression to equation 8, where the solid conductivity ($k_p$, Appendix C) was used instead of $k_{e,r}$. With respect to the diffusion of the gases in the tablet, the bulk diffusion by Stefan–Maxwell equations and the Knudsen diffusion were considered for estimating the intraparticle diffusion limitations, which is expressed by the species equations [47, 52]:

$$-\nabla \cdot \boldsymbol{J_i} + S_i = \rho D_{i,eff} \nabla Y_i + S_i = 0 \tag{10}$$

$$D_{i,eff} = (\varepsilon/\tau)(1/D_{i,eff,S} + 1/D_{i,K})^{-1} \tag{11}$$

where $i$ represents the $i^{th}$ species; $Y$ is the mass fraction; $D_{i,eff,S}$ is the

effective diffusivity based on the Maxwell–Stefan equations (Appendix D); $D_{i,K}$ is the Knudsen diffusion coefficient (Appendix D); $\varepsilon$ is the porosity of the catalyst, $\tau$ is the tortuosity of pores in the catalyst, and the $\varepsilon/\tau$ ratio of 0.123 [50] was employed in this study; $S_i$ (kg/m$^3\cdot$ s) is the source term, and the $S_i$ values for the four independent species ($CO_2, H_2, H_2O$ and MeOH) for the species equations are calculated by

$$S_{CO_2} = -\rho_{cat}(r_{MeOH} + r_{RWGS})M_{CO_2} \tag{12}$$

$$S_{H_2} = \rho_{cat}(-3r_{MeOH} - r_{RWGS})M_{H_2} \tag{13}$$

$$S_{H_2O} = \rho_{cat}(r_{MeOH} + r_{RWGS})M_{H_2O} \tag{14}$$

$$S_{MeOH} = \rho_{cat} r_{MeOH} M_{MeOH} \tag{15}$$

where $M$ is the molecular weight for each species. The mass fraction of the component CO was calculated by

$$\sum_{i=0}^{4} Y_i = 1 \tag{16}$$

The effectiveness factor of the catalyst tablet for reaction (2) or (3) was calculated by

$$\eta = \frac{R_t}{R_s} = \frac{\int_0^V r_t dv}{\int_0^V r_s dv} \tag{17}$$

where $R_t$ and $r_t$ are the total reaction rate and reaction rate of reaction (2) or (3) in the tablet, respectively, $R_s$ and $r_s$ are the total reaction rate

and reaction rate calculated based on the conditions on the tablet surface, respectively, and $V$ is the volume of the catalyst tablet. Along the catalyst bed with a length of L, the average effectiveness factor was calculated and used for the pseudo-homogeneous model, which was expressed by

$$\eta_{avg} = \frac{\int_0^L R_t dl}{\int_0^L R_s dl} \tag{18}$$

## 3. Results and discussions

### *3.1. Adiabatic reactor*

#### *3.1.1. Single-pass process*

The adiabatic reactors designed for the STM process usually comprise multiple catalyst beds. Cooling methods such as injection of quench (cold) gas are employed to decrease the gas temperature after each bed to avoid undesirable hot-spot temperatures in the catalyst bed which can result in the catalyst deactivation by sintering. The temperature increase in each catalyst bed is attributed to the exothermic reactions (1) and (2). For the CTM process, however, with more involvement of reaction (2) (the main reaction) and the endothermic reaction (3), the reaction heat released in the process is much lower than that from the STM process, which indicates a milder temperature increase in the catalyst bed. Figure 3(a) shows the equilibrium outlet temperature ($T_{out}$) for a single-pass methanol synthesis process with different SN values and CO contents, the Gibbs reactor in Aspen Plus is used for the calculation. $T_{out}$ is also the hot-spot temperature assuming a single-bed adiabatic reactor was used. Relatively low outlet temperatures are achieved when the CO content is lower in the feed gas, e.g., when $CO/(CO+CO_2)<0.2$, $T_{out}$

is less than 282 °C which is close to the temperature range (220–280 °C) [6] for the conventional STM process. This also indicates the potential to use a simple and low-cost single-bed adiabatic reactor for the CTM process assuming similar catalyst stability to that in the STM process. Additionally, the SN value is usually higher than 2 for the stream (stream S3, in Fig. 1) at the inlet of the reactor (due to the recycling of the product stream, see Section 3.1.2), which can further decrease the outlet temperature, e.g., $T_{out}$ is 275 °C when $CO/(CO+CO_2)$=0.2 and SN=8. The methanol (MeOH) yield for the adiabatic condition is also presented as shown in Figure 3(b). Presumably, a high CO content is more favorable for methanol synthesis under the similar pressure and temperature conditions [42]. However, for the adiabatic conditions, the relatively high CO content in the feed gas also results in high outlet temperatures, which are not favorable for the exothermic methanol synthesis reactions. Consequently, a decreasing trend of methanol yield with increasing CO content is observed, as shown in Figure 3(b).

Compared with the STM process, the RWGS reaction exerts a higher influence on the CTM process due to the higher $CO_2$ content in the feed gas, which can result in a retarded increase or even decrease in the temperature along the reactor tube. The effect of the inlet temperature and operating pressure (the operating pressure of the Gibbs reactor equals the pressure of the feed gas) are also investigated as shown in Figure 4 for the adiabatic CTM process. The outlet temperature and temperature difference ($\Delta T = T_{out}$-$T_{in}$) increased and decreased with the rising inlet temperature. The latter trend is attributed to the more favorable endothermic RWGS reaction at relatively high temperatures, and a negative value of $\Delta T$ was found

for the condition of 30 bar, e.g., $\Delta T = -6.3\,^{\circ}C$ with $T_{in} = 270\,^{\circ}C$ and P=30 bar. The high operating pressures result in high outlet temperatures (or hot-spot temperatures) due to the promoted exothermic methanol synthesis reactions; therefore a low $T_{in}$ is required for the high-pressure conditions; for instance, for $T_{out} < 280\,^{\circ}C$, $T_{in} < 220\,^{\circ}C$ is required for the condition of P= 80 bar, which leaves a narrow range of $T_{in}$. For the conditions of P= 30 bar and P= 50 bar $T_{out} < 280\,^{\circ}C$ is fulfilled for most of the $T_{in}$ values, which indicates a higher operating flexibility under these conditions. The influences of the inlet temperature and pressure on the methanol yield are also considered, as shown in Figure 4(b). The methanol yield decreases with increasing $T_{in}$ at different pressures, which is attributed to both the promotion of the RWGS reaction and the depression of the methanol synthesis reactions by relatively high temperatures and low pressures.

*3.1.2. Process with the recycle stream*

Similar to the conventional STM process, the CTM process requires the recycling of the unconverted feed gas with certain recycling ratios (N, the mole ratio of the recycled stream/feed gas) due to the low single-pass conversion of this process. As shown in Fig. 1(a), the components of methanol and water in stream S4 were further condensed and separated through an ideal gas/liquid separator at a typical operating temperature of 40 °C and an assumed pressure drop of 2 bar between the separator and the reactor. A small portion of the gas from the separator was purged to avoid the accumulation of inert gases (e.g., $N_2$) in the system; the remainder was compressed to the operating pressure, and returned to the methanol synthesis process as the recycle stream (stream S9); 99.9% of the unconverted gas was recy-

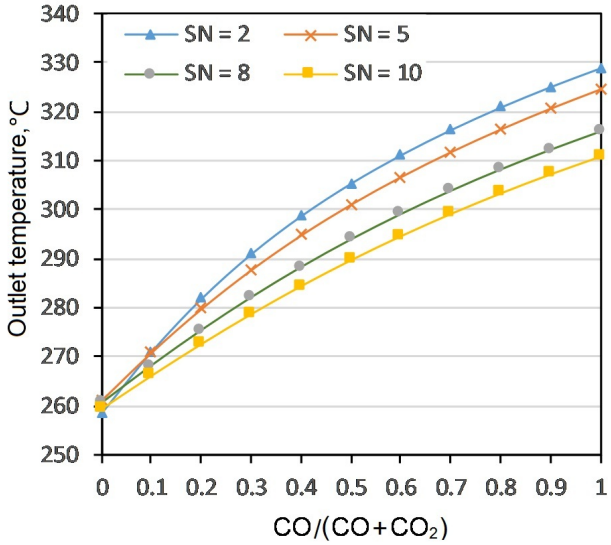


(a)

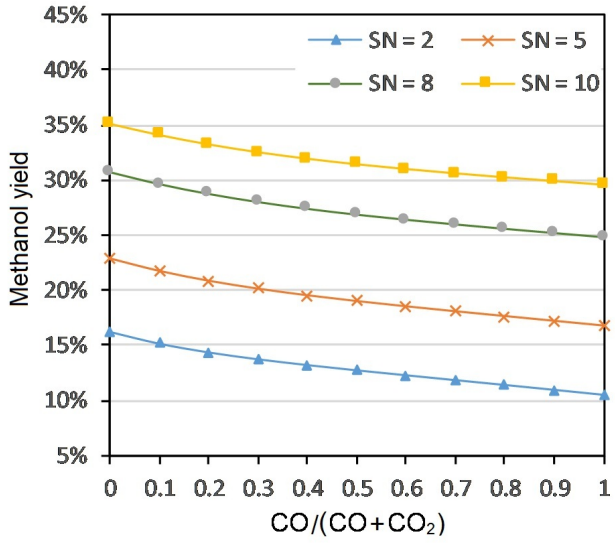


(b)

Figure 3: Equilibrium (a) outlet temperature and (b) methanol yield for the adiabatic CTM and STM processes at P= 50 bar, $T_{in}$= 210 °C, and different SN values and CO content.

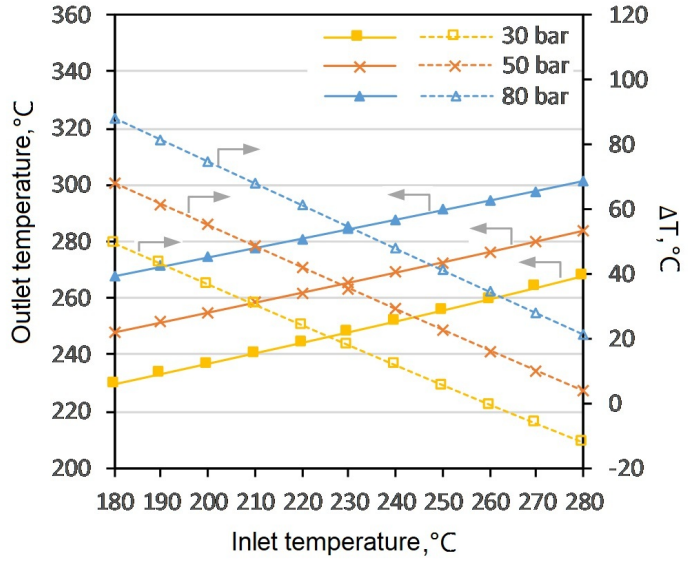


(a)

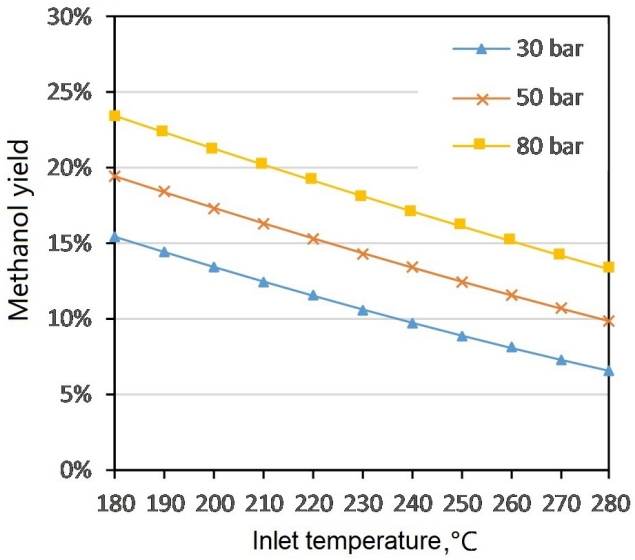


(b)

Figure 4: Equilibrium (a) outlet temperature and (b) methanol yield for the adiabatic CTM process at SN= 2; different pressures and inlet temperatures.

cled to achieve a high methanol yield (larger than 98% in the simulations of this study), which is required for running a methanol plant to minimize the waste of feed gases. A higher value of this recycle factor (larger than 99.9%) has also been tried for a higher methanol yield (e.g., 99%), which caused convergence problem for most of the simulations in this study. The temperature of the feed stream (stream S3) at the inlet of the reactor was set at 210 °C, which is a typical inlet temperature for a industrial methanol reactor, a higher inlet temperature can result in a higher outlet temperature (hot-spot temperature) and a lower methanol yield as shown in Figure 4 for the adiabatic CTM process. Moreover, there is requirement of the lower limit for $T_{in}$ by the commercial copper-based catalysts, e.g., 190 °C for the Topsøe MK-121 catalyst.

The simulations were conducted at different operating pressures (30–80 bar) to investigate the potential of the adiabatic CTM process. The simulation results were shown in Table S3 (Appendix B), Compared with feed stream S1, there are certain amounts of CO component and high $H_2$ contents in stream S3, which were influenced by the recycle stream and result in $CO/(CO+CO_2)$ ratios of 0.21, 0.18, and 0.15 and SN values of 6.13, 8.27, and 9.48 for the conditions of P= 30, 50, and 80 bar, respectively. The key performance indicators were shown in Table 1, where the hot-spot temperature $T_{max}$ is also the outlet temperatures for the adiabatic reactor. Due to that the methanol synthesis reaction favors high pressure, the cases with higher operating pressures resulted in higher one-pass methanol yields, lower recycle ratios and higher $T_{max}$ values. The $T_{max}$ values of were below or slightly higher than the conventional upper limit of 280 °C, which indicates

the potential of the application of a single-bed adiabatic reactor to the CTM process.

Additionally, the potential of a single-bed adiabatic reactor to be employed for the STM process with a $CO_2$–rich feed gas (at the reactor inlet) was also investigated. Figure 5 shows the equilibrium outlet temperature for the adiabatic CTM and STM processes with a recycle stream at different operating pressures for the reactor and different CO contents ($CO/(CO+CO_2)$ ratios) for feed stream S1. The maximum operating pressure decreased with the increase in the CO content in stream S1. For a typical syngas CO content of $CO/(CO+CO_2)= 0.5$, P<40 bar is required assuming $T_{max}$ is less than 280 °C, which indicates a low feasibility for the application of the adiabatic reactor at a high operating pressure (i.e., larger than 40 bar).

Table 1: Key performance indicators for the adiabatic CTM process with the recycle stream under different pressures

| | **P = 30bar** | **P = 50bar** | **P = 80bar** |
|---|---|---|---|
| $T_{max}$, °C | 254.9 | 269.5 | 284.3 |
| Recycle ratio | 9.5 | 7.2 | 5.7 |
| Single-pass methanol yield | 18.7% | 30.7% | 41.9% |

### *3.2. Water-cooled reactor*

The water-cooled reactor or boiling water reactor with a shell-tube structure is widely used for methanol production. The evaporation of the boiling water in the shell side provides an efficient method for removing the reaction heat from the exothermic STM process in the tube side. Additionally, the hot-spot temperature along the reactor tube can be limited to an acceptable value (e.g., 280 °C). For the CTM process, these hot-spot temperatures are

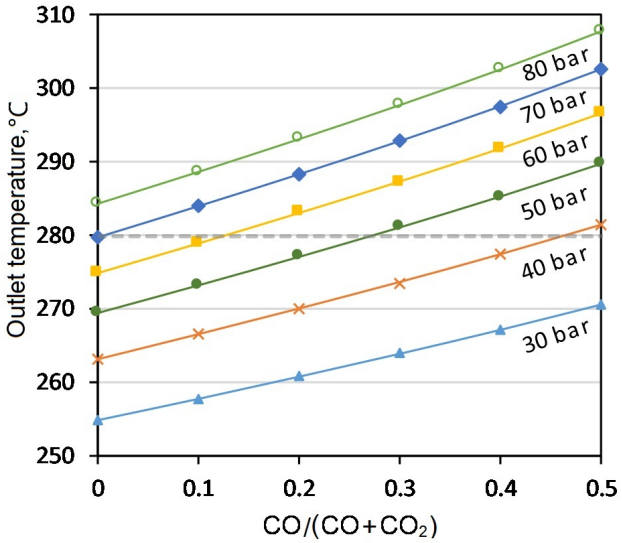


Figure 5: Equilibrium outlet temperature for the adiabatic CTM and STM processes with a recycle stream; SN= 2, $T_{in}$=210 °C and different operating pressures for the reactor, and different CO contents ($CO/(CO+CO_2)$) for feed stream S1 are employed.

supposed to be lower due to the low intensity of the heat released compared with that in the STM process. In this study, the condition with the recycle stream was calculated for the CTM and STM processes with water-cooled reactors (Fig. 1(b)). $T_{in}$=210 °C and the same conditions as those mentioned in Section 3.1.2 for the gas/liquid separator were set. A typical temperature of 250 °C was set for the boiling water in the reactor. The conditions with high pressures of 50–80 bar were considered in this section, which have higher outlet temperatures than the conditions with 30 bar (see Table 1), in addition to a high potential for improvement using the water-cooled reactor.

Figure 6 shows the temperature and methanol yield along the reactor length with different operating pressures and $CO/CO_2$ ratios for feed stream S1. The higher CO contents for the STM process results in higher methanol yields than those for the CTM process, which indicates a higher reaction rate for the MeOH synthesis with a higher CO content in feed stream S1 under the investigated conditions. Significant temperature increments were observed near the inlet, where the feed gas could be heated by both the boiling water and the heat released by the exothermic methanol synthesis reactions. The temperature rise also accelerated the reaction rates and generated more heat, which was absorbed by the boiling water. Hot-spots were achieved in the reactor when the reaction heat released was equal to the heat transfer rate between the gas phase in the tube side and the boiling water in the shell side of the reactor. The temperatures of the hot-spots (A–F, shown in Figure 6) are 256 °C, 263 °C, 271 °C, 257 °C, 268 °C and 280 °C for the CTM and STM processes with typical $CO/CO_2$ ratios, respectively. Compared with the STM process, the CTM process has a mild temperature distribution and

lower hot-spot temperature in the reactor. For the STM process, the hot-spot temperature ($T_{max}$) increased by 5–9 °C with increasing pressures of 50–80 bar, whereas $T_{max}$ increased by only 1 °C for the CTM process. In addition, the $T_{max}$ values for the CTM process are 7–23 °C lower than those for the STM process, which can further decrease the detrimental thermal effect (sintering of copper) on the conventional copper-based catalyst used for the methanol synthesis process.

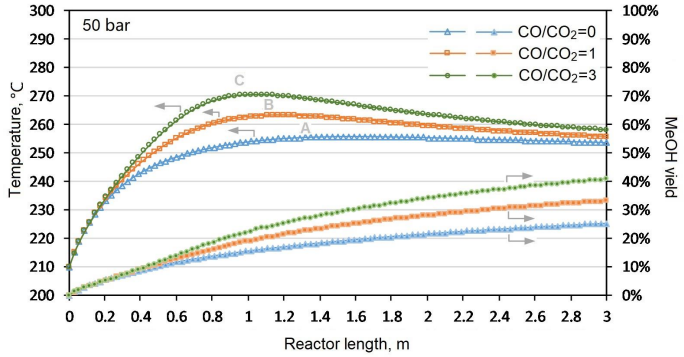


(a)

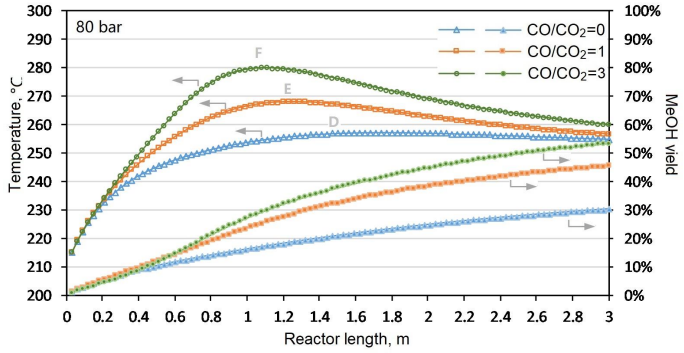


(b)

Figure 6: Temperature and methanol yield along the water-cooled reactor at P=50–80 bar, $T_{in}$=210 °C and different $CO/CO_2$ ratios for feed stream S1.

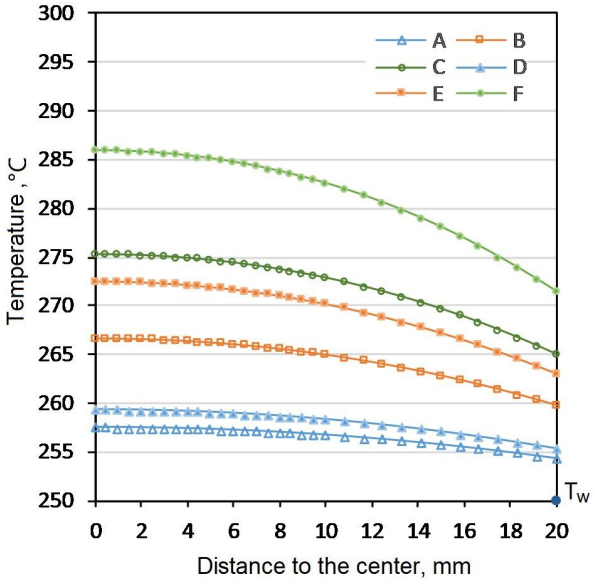


(a)

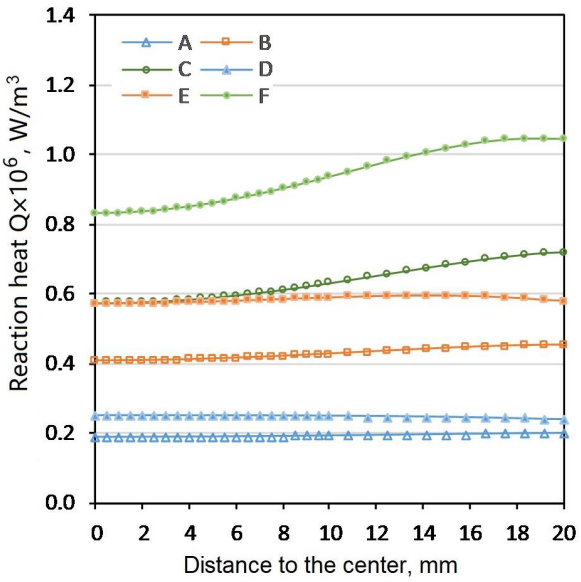


(b)

Figure 7: (a) Radial temperature profile and (b) reaction heat at the cross-sections (A–F).

Temperature gradients also exist in the radial direction in the packed-bed reactor tube; consequently, a higher local hot-spot temperature could be achieved at the tube center than the average temperatures calculated by the pseudo-homogeneous model. The radial heat transfers at the cross-sections of A–F (hot-spots in Figure 6, hereinafter referred to as A–F) were also considered by CFD modeling to compare the center temperatures ($T_c$) for the STM and CTM processes, where the heat transfer rate between the boiling water and the gas phase equals the rate of heat released in the tube side. The required parameters for the CFD model and the calculated average temperatures for A–F by the CFD model ($T_1$) and pseudo-homogeneous model ($T_2$) are shown in Table S4 (Appendix C), where light differences can be found between the $T_1$ and $T_2$ values predicted by the two methods. The temperature profiles in the radial direction at A–F are shown in Figure 7(a). From the outer wall ($T_w$=250 °C) to the tube center, there are relatively low temperature increments (7.5 °C and 9.3 °C for A and D, respectively) for the CTM process, whereas noticeably high temperature increments are achieved for the STM process, e.g., 16.7 °C, 25.3 °C, 22.5 °C, and 36.0 °C for B, C, E, and F, respectively, which agrees with the trends in Figure 6 by the pseudo-homogeneous model. The center temperatures ($T_c$) are slightly higher than the average hot-spot temperatures ($T_{max}$) calculated by the pseudo-homogeneous model. These temperature differences can be neglected for the CTM process (1.5–2.3 °C) but may need to be taken into account for the STM process (3.7–6.0 °C).

Additionally, compared with the mild temperature change in the bulk packed bed, around 60% of the temperature increases were represented by

the temperature jumps (at the wall) in the present model due to the low $h_w$ values (i.e., high heat resistance for the near-wall region). For the bulk packed bed, the temperature change is large near the wall and small near the tube center as shown in Figure 7(a), which is mainly attributed to the lower reaction heat released near tube center. The trend of the reaction heat in the radial direction is also shown in Figure 7(b) where the reaction heats are intense near the wall for the STM process with a high CO content (B, C and F), while the trends for other cross-sections were not obvious. The trends of the reaction heat in the radial reaction is attributed to the balance of the endothermic RWGS reaction and the exothermic methanol synthesis reaction. In addition, the high temperature is unfavorable for the MeOH synthesis reactions, which may decrease the distance to the equilibrium and reaction rates. Notably, the radial mass transfer in the packed bed was not considered in the study, which may slightly influence the trends.

With respect to the tube diameter designed for the STM process, a small tube diameter (typically around 40 mm [53]) is usually used in the industry to provide a sufficient heat exchanging area for the strongly exothermic STM process and a reasonable reactor volume as well as an acceptable center temperature in the tube. For the CTM process or STM process with $CO_2$–rich feed gas, this diameter could be adjusted (e.g., using a larger tube) due to the relatively low reaction heat released. Similar to the cross-sections A–C in Figure 7, a large tube diameter of 100 mm was considered, and the radial temperature and reaction heat for the hot-spots (cross-sections) with different $CO/CO_2$ ratios for feed stream S1 (in Figure 1(a)) and P= 50 bar are shown in Figure S1 (Appendix C). The trends are similar to those (cross-sections,

A–C) in Figure 7, but show higher center temperatures. However, the $T_c$ values are still within the conventional temperature range (220–280 °C) for the conditions of $CO/CO_2$=0–1, which indicates that compared with the traditional STM process the range of the tube diameter for the CTM process or STM process with $CO_2$–rich feed gas could be expanded.

### *3.3. Gas-cooled reactor*

The typical structure of a gas-cooled methanol reactor is shown in Figure 1(b), where the catalyst bed is in the shell side and cooled by the cold feed in the tube side. Compared with the water-cooled reactor, the gas-cooled reactor is less complex without the introduction of an additional water stream. Similar to the study on the water-cooled reactor, the condition with the recycle stream was calculated for the CTM and STM processes with gas-cooled reactors (shown in Figure 1(a)). The $T_{in}$ values of 210 °C and 235 °C and the same conditions as those mentioned in Section 3.1.2 for the gas/liquid separator were set. The outlet temperature of the cold feed (stream C2) was set equal to that at the inlet of the catalyst bed (stream S3), and the composition of the cold feed (stream C1) was set equal to that of stream S3. The operating pressure of 50 bar was considered in this section. A tube diameter of 25 mm was assumed for the tube side. The catalyst bed in the shell side was approximated by a multi-tube structure with a tube diameter of 58–60 mm . The tube number was adjusted to achieve a GHSV value close to 10000 $h^{-1}$ for the catalyst bed.

Figure 8 shows the temperature and methanol yield in the gas-cooled reactor for the CTM and STM processes. The trends of the temperature in Figure 8(a) and methanol yield in Figure 8(c) are similar to those for

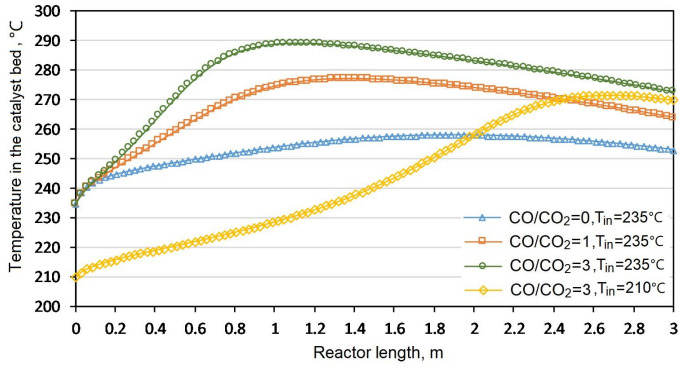


(a)

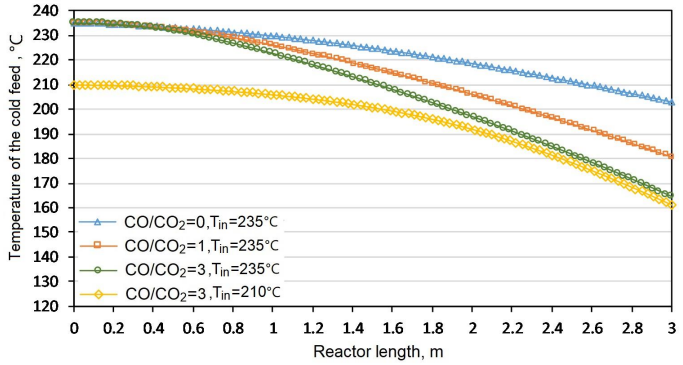


(b)

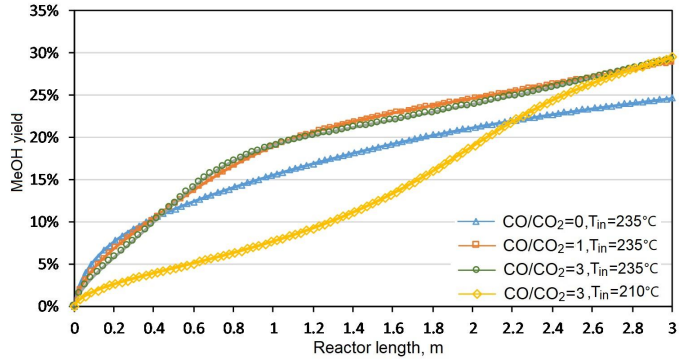


(c)

Figure 8: Temperature of the catalyst bed, cold feed, and methanol yield in the gas-cooled reactor at P=50 bar, $T_{in}$=210–235 °C, and different $CO/CO_2$ ratios for feed stream S1.

the water-cooled reactor in Figure 6. Additionally, the temperature of the cold feed is shown in Figure 8(b) where the cold feed was heated by the gas phase in the shell side and the temperatures of stream C1 were determined to be from 161.2 °C to 203.0 °C. The temperature of the tube side near the inlet of the catalyst bed (e.g., 0–0.1m) is close to (or lower than) that in the shell side; therefore, the temperature increase (Figure 8(c)) in this area is mainly attributed to the exothermic reactions, which is different from the condition for a water-gas reactor where the gas phase can also be heated by the boiling water. Consequently, a higher $T_{in}$ value could be required for a gas-cool reactor to avoid an extremely low reaction rate near the inlet of the catalyst bed; for instance, a $T_{in}$ value of 210 °C for the CTM process ($CO/CO_2$=0) results in a very low $T_{out}$ value of less than 230 °C and $y_{MeOH}$ of less than 15% (not shown in Figure 8). Therefore, a higher "ignition" temperature ($T_{in}$) is required for the CTM process using a gas-cooled reactor. For the STM processes, there is no "ignition" problem with $T_{in}$=210 °C, i.e., for the condition of $CO/CO_2$=3 and $T_{in}$=210 °C shown in Figure 8(a), a hot-spot temperature of 271.8 °C was achieved. Similar to the trends for the water-cooled reactor(shown in Figure 6(a)), there is a mild temperature distribution for the CTM process in the gas-cooled reactor and a lower hot-spot temperature (258.2 °C) than those for the STM process (271.8–289.3 °C). These local hot-spot temperatures in the "radial" direction of catalyst bed are slightly higher than the $T_{max}$ values, which may also need to be taken into account (Figure S2, Appendix C).

*3.4. Comparison of the three reactors types*

The main difference of the three reactor types mentioned above is related to the method of heat removal in the reactors. The main concerns include a proper hot-spot temperature (e.g., less than 280 °C), and a reasonable single-pass methanol yield for a certain catalyst volume. The latter is determined by the reaction rate (per volume catalyst) as well as the temperature profile along the reactor.

For the traditional STM process with a high CO content (e.g., $CO/CO_2$=3) the design of a single adiabatic reactor is only feasible at low operating pressures, e.g., P<30 bar. For higher operating pressures, a traditional multi-bed or multi-reactor design with internal or external cooling is required to limit the $T_{max}$ value for the process. Compared with the adiabatic reactor, the gas-cooled reactor can provide a way of heat removal for the catalyst bed, however, the gas-cooled reactor need a high "ignition" temperature at the inlet (see section 3.3), which still results in a hot-spot temperature higher than the conventional range, e.g., $T_{max}$=289.3 °C with P= 50 bar, $CO/CO_2$= 3, and $T_{in}$=235 °C (shown in Figure 8(a)). The water-cooled reactor showed a more efficient way of heat removal and higher methanol yield than the gas-cooled reactor by comparing the simulation results in Figure 6 with those in Figure 8. This results agree with wide application of the water-cooled reactor in the market for the traditional methanol production. For the STM process with a $CO_2$-rich feed gas ($CO/CO_2$= 1), the application of the adiabatic reactor still exhibited low feasibility as mentioned in Section 3.1.2, and gas-cooled reactor shows feasibility at low and medium pressures, e.g., P<50 bar.

Table 2: The key operating and design parameters for the three reactor types

| **50 bar** | **Adiabatic** | **Water-cooled** | **Gas-cooled** |
|---|---|---|---|
| Stream S1 | | | |
| $H_2$, kmol/h | 48 | 48 | 48 |
| $CO_2$, kmol/h | 16 | 16 | 16 |
| $T_{in}$, °C | 215 | 210 | 235 |
| Operating Pressure, bar | 50 | 50 | 50 |
| Tube I.D., $mm$ | | 40 | 25 |
| Tube O.D., $mm$ | | 44 | 29 |
| Tube number | | 347 | 330 |
| Reactor I.D., $m$ | 0.745 | 1.418 | 0.913 |
| Reactor length $m$ | 3 | 3 | 3 |
| Catalyst volume, $m^3$ | 1.31 | 1.31 | 1.31 |
| GHSV, $h^{-1}$ | 10686 | 10402 | 10484 |
| Heat transfer coefficient, $W/m^2 \cdot K$ | | 321.7 | 60.4 |

With respect to the CTM process, all the three reactor types showed potentials as mentioned in the above sections. The condition with the recycle stream was calculated for the CTM processes with the three reactor types by the pseudo-homogeneous model as shown in Figure 1(a). The $T_{in}$ values of 210–235 °C and the same conditions as those mentioned in Section 3.1.2 for the gas/liquid separator were set. The key operating and design parameters for the three reactors were given in Table 2. The effectiveness factors for the catalyst bed in the three reactors by the 2-D CFD model (Section 2.3) were investigated combined with the pseudo-homogeneous model. The trends of the effectiveness factors in the reactors under the conditions given by Table 2 were demonstrated in Figure 9(a). The water-cooled and gas-cooled reactor show very similar trends of the $\eta_{MeOH}$ value, while the adiabatic reactor

exhibits a higher value in the in the middle part of the reactor (0.4–2.4 m). The average effectiveness factor for the adiabatic reactor, water-cooled reactor and gas-cooled reactor are 0.56, 0.46, and 0.42, respectively. The effectiveness factors of the RWGS reaction (reaction (3)) in the three reactor types are shown in Figure 9(b). There are hyperbolic trends found for all the three cases with large positive ($> 1.0$) and negative values. These trends are due to that the direction of the RWGS reaction is reversed to the water gas shift (WGS) reaction along the reactors, which occurs faster inside the catalyst tablet than that on the tablet surface.

Table 3: Key performance indicators for the adiabatic CTM process with the recycle stream and different reactors

| **P= 50 bar** | **Adiabatic** | **Water-cooled** | **Gas-cooled** |
|---|---|---|---|
| $T_{max}$, °C | 264.5 | 256.0 | 258.2 |
| Recycle ratio | 8.8 | 8.5 | 8.6 |
| Single-pass methanol yield | 23.6% | 25.0% | 24.6% |

Additionally, the key performance indicators for the three reactors in the CTM process were presented in Table 3. The water-cooled reactor exhibited slightly higher performance with a lower hot-spot temperature, which can be attributed to its more efficient way of heat removal compared with the other two reactors, e.g., a higher heat transfer coefficient of 321.7 $W/m^2 \cdot K$ (shown in Table 2). The efficient heat removal can also beneficial for the conditions with temperature fluctuations at the reactor inlet, where a too-low $T_{in}$ can be increased by the boiling water (e.g., 250 °C) and the intensive reaction heat caused by a too-high $T_{in}$ can also be efficiently removed by the boiling water. As shown in Table 3, the adiabatic reactor presented a lower single-pass methanol yield and a higher recycle ratio, this trend is more obvious at

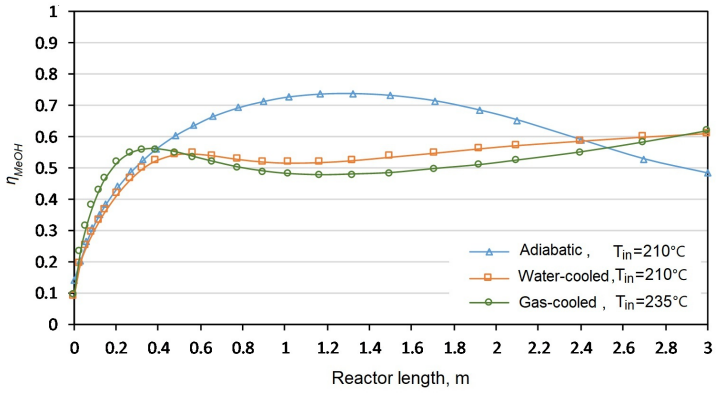


(a)

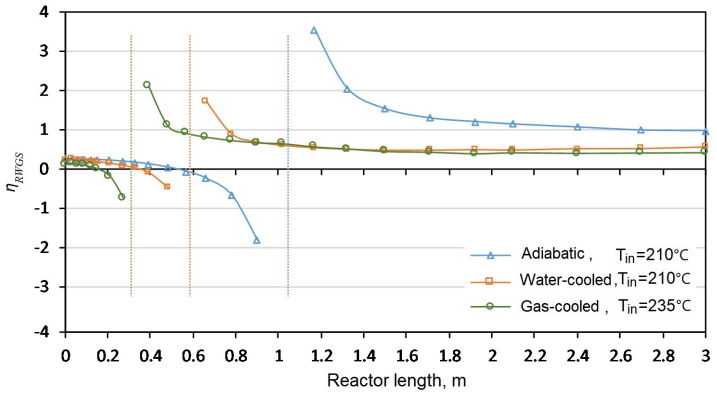


(b)

Figure 9: The effectiveness factor of (a) reaction (2) and (b) reaction (3) at P=50 bar, $T_{in}$=210–235 °C, and in different reactor types for the CTM process.

a higher operating pressure of 80 bar (Table S5, Appendix E). In addition, a higher "ignition" temperature ($T_{in}$=215 °C) is required (shown in Table 2) for the adiabatic reactor, which indicates a narrower range for the $T_{in}$ value compared with that for the water-cooled reactor. With respect to the gas-cooled reactor, it exhibits similar performance to that for the water-cooled reactor (shown in Table 2) but has a smaller reactor diameter (or volume) which is attributed to the relatively high catalyst loading in the shell side and a smaller tube diameter (for the cold feed). The heat-couple design of the gas-cooled reactor can also decease the load (or size) of the heat exchangers for preheating the feed. The disadvantages of this reactor could be the possible non-uniform distribution of the gas flow and temperature in the shell side where a properly designed distributor is desired. Additionally, a relatively high $T_{in}$ value (e.g., $T_{in}$= 235 °C as shown in Table 2) is required for the reactor, which would result in a slightly increased hot-spot temperature and a narrower range of the $T_{in}$ value.

Furthermore, besides the KPIs mentioned in Table 3, the reactor cost is also an important factor for the applications of the reactors. The capital costs for the CTM process (Figure S3, Appendix F) with the three reactor types were evaluated by [54]

$$C_c = C_B(Q_c/Q_B)^M f_M f_P f_T \tag{19}$$

where $C_B$ and $Q_B$ are the base cost and base capacity, respectively, $Q_C$ is the design component capacity, M is the cost exponent, $f_M$, $f_P$ and $f_T$ are the material of construction capital cost factor, pressure correction factor and temperature correction factor, respectively. The capital cost for the

components of the reactors, heat exchangers, compressor and flash tanks were calculated by equation 19.The parameter values for the calculations can be found in Appendix F.

The capital cost estimation for CTM process with three reactors and different operating pressures were presented in Figure 10. The differences of the total capital cost are mainly attributed by the differences of the reactor capital cost, and the total values for other capital costs are around 180,000–220,000 $ for all the cases. The water-gas reactor shows the highest reactor capital costs at the two pressures, which is attributed to its larger tube diameter and reactor diameter (shown in Table 2). The adiabatic reactor exhibits the lowest reactor cost due to its simpler structure and smaller reactor diameter, and the gas-cooled reactor presents a medium cost level.

## 4. Conclusions

A comparative study was conducted on the adiabatic, water-cooled and gas-cooled reactors for the methanol synthesis from syngas and $CO_2$ under the conditions of $T_{in}$= 180-280 °C, P= 30-80 bar, feed gases of SN= 2–10 and $CO/(CO+CO_2)$= 0-1. The temperature profiles in the axial and radial directions, particularly the hot-spot temperatures, operating conditions and methanol yields for the reactors have been investigated using thermodynamic analysis, the CFD method and the pseudo-homogeneous model. The capital costs for CTM process with the three reactor types have also been evaluated.

Compared with the traditional STM process with a high CO content (e.g., $CO/CO_2$= 3), the STM process with a $CO_2$–rich feed gas and the CTM process exhibited reduced hot-spot temperatures from a thermodynamic point of

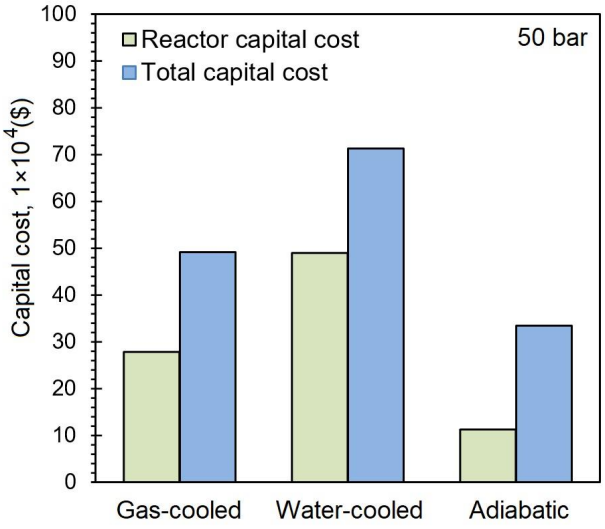


(a)

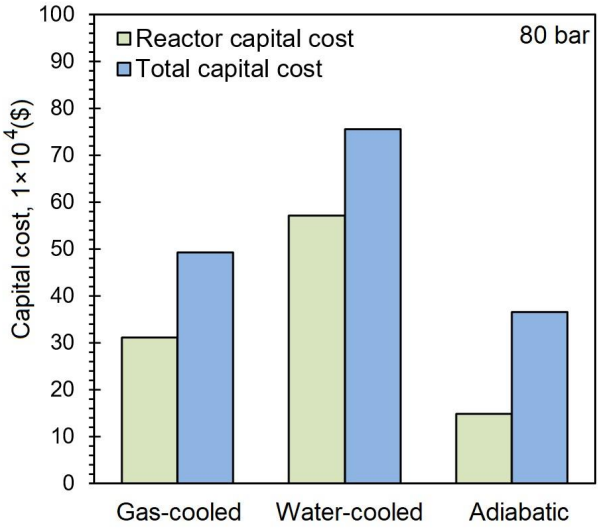


(b)

Figure 10: The capital cost for the CTM process with different reactor types and operating pressures of (a) P= 50 bar and (b) P= 80 bar.

view. Consequently, besides the widely used water-cooled reactor the single-bed adiabatic (without internal cooling) reactor and the gas-cooled reactor also exhibited potentials for the CTM process, where the hot-spot temperatures in the reactors can be within the typical operating temperature range for the catalyst. For the STM process with the $CO_2$–rich feed gas, single-bed adiabatic (without internal cooling) reactor and the gas-cooled reactor only showed feasibility at low or medium pressure (e.g.,P$<$ 50 bar).

With respect to the comparison of the three reactor types for the CTM process, all the three reactor types demonstrated similar trends of the effectiveness factor of the catalyst with approximated range 0.4–0.6 for the methanol synthesis reaction and 0.2–0.4 for the RWGS (or WGS) reaction under the investigated conditions. The water-cooled reactor showed advantages in terms of efficient heat removal, low hot-spot temperature and wide relatively range inlet temperature for control.

The adiabatic reactor and the gas-cooled reactor demonstrated a relatively low and medium performance (hot-spot temperature, recycle ratio and single-pass methanol yield), respectively. However, the same trends of capital cost were also found for the three reactors, which indicates the potentials for the adiabatic reactor and gas-cooled reactor types in a small-scale CTM process.

**Acknowledgement**

The authors would like to acknowledge support of this work from the Danish Energy Agency (EUDP) funded projects Cryogenic Carbon Capture and Use (C3U, grant number—64017-0026)) and Power2Met (grant number—

64018-0552).

## References

[1] S. Al Shakhshir, X. Cui, S. Frensch, S. K. Kær, In-situ experimental characterization of the clamping pressure effects on low temperature polymer electrolyte membrane electrolysis, International Journal of Hydrogen Energy 42 (2017) 21597–21606.

[2] M. David, C. Ocampo-Martínez, R. Sánchez-Peña, Advances in alkaline water electrolyzers: A review, Journal of Energy Storage 23 (2019) 392–403.

[3] G. A. Olah, A. Goeppert, G. K. S. Prakash, Beyond Oil and Gas : The Methanol Economy, Wiley & Sons, 3rd edition, 2018.

[4] F. Pontzen, W. Liebner, V. Gronemann, M. Rothaemel, B. Ahlers, $CO_2$-based methanol and DME - Efficient technologies for industrial scale production, Catalysis Today 171 (2011) 242–250.

[5] É. S. Van-Dal, C. Bouallou, Design and simulation of a methanol production plant from $CO_2$ hydrogenation, Journal of Cleaner Production 57 (2013) 38–45.

[6] M. Bertau, H. Offermanns, L. Plass, F. Schmidt, H.-J. Wernicke (Eds.), Methanol: The basic chemical and energy feedstock of the future: Asingers vision today, Springer-Verlag Berlin Heidelberg, 1 edition, 2014.

[7] S. G. Jadhav, P. D. Vaidya, B. M. Bhanage, J. B. Joshi, Catalytic carbon dioxide hydrogenation to methanol: A review of recent studies, Chemical Engineering Research and Design 92 (2014) 2557–2567.

[8] M. Pérez-Fortes, J. C. Schöneberger, A. Boulamanti, E. Tzimas, Methanol synthesis using captured $CO_2$ as raw material: Techno-economic and environmental assessment, Applied Energy 161 (2016) 718–732.

[9] S. Brynolf, M. Taljegard, M. Grahn, J. Hansson, Electrofuels for the transport sector: A review of production costs, Renewable and Sustainable Energy Reviews 81 (2018) 1887–1905.

[10] D. S. Marlin, E. Sarron, . Sigurbjörnsson, Process Advantages of Direct $CO_2$ to Methanol Synthesis, Frontiers in Chemistry 6 (2018) 1–8.

[11] S. S. Araya, V. Liso, X. Cui, N. Li, J. Zhu, S. L. Sahlin, S. H. Jensen, M. P. Nielsen, S. K. Kær, A Review of The Methanol Economy: The Fuel Cell Route, Energies 2020, Vol. 13, Page 596 13 (2020) 596.

[12] B. Hu, C. Guild, S. L. Suib, Thermal, electrochemical, and photochemical conversion of $CO_2$ to fuels and value-added products, Journal of CO2 Utilization 1 (2013) 18–27.

[13] K. A. Ali, A. Z. Abdullah, A. R. Mohamed, Recent development in catalytic technologies for methanol synthesis from renewable sources: A critical review, Renewable and Sustainable Energy Reviews 44 (2015) 508–518.

[14] M. De Falco, M. Capocelli, Direct Synthesis of Methanol and Dimethyl Ether From a $CO_2$-Rich Feedstock: Thermodynamic Analysis and Selective Membrane Application, Methanol (2018) 113–128.

[15] Y. Jiang, H. Yang, P. Gao, X. Li, J. Zhang, H. Liu, H. Wang, W. Wei, Y. Sun, Slurry methanol synthesis from $CO_2$ hydrogenation over microspherical SiO2 support Cu/ZnO catalysts, Journal of CO2 Utilization 26 (2018) 642–651.

[16] M. Bukhtiyarova, T. Lunkenbein, K. Kähler, R. Schlögl, Methanol Synthesis from Industrial $CO_2$ Sources: A Contribution to Chemical Energy Conversion, Catalysis Letters 147 (2017) 416–427.

[17] O. S. Joo, K. D. Jung, I. Moon, A. Y. Rozovskii, G. I. Lin, S. H. Han, S. J. Uhm, Carbon dioxide hydrogenation to form methanol via a reverse-water-gas- shift reaction (the CAMERE process), Industrial and Engineering Chemistry Research 38 (1999) 1808–1812.

[18] F. Gallucci, L. Paturzo, A. Basile, An experimental study of $CO_2$ hydrogenation into methanol involving a zeolite membrane reactor, Chemical Engineering and Processing: Process Intensification 43 (2004) 1029–1036.

[19] A. Zachopoulos, E. Heracleous, Overcoming the equilibrium barriers of $CO_2$ hydrogenation to methanol via water sorption: A thermodynamic analysis, Journal of CO2 Utilization 21 (2017) 360–367.

[20] A. Arora, S. S. Iyer, I. Bajaj, M. M. Faruque Hasan, Optimal Methanol

Production via Sorption-Enhanced Reaction Process, Industrial and Engineering Chemistry Research 57 (2018) 14143–14161.

[21] X. Cui, S. K. Kær, Thermodynamic analyses of a moderate-temperature carbon dioxide hydrogenation to methanol via reverse water gas shift process with in situ water removal, Industrial & Engineering Chemistry Research 58 (2019) 10559–10569.

[22] M. Bukhtiyarova, T. Lunkenbein, K. Kähler, R. Schlögl, Methanol Synthesis from Industrial $CO_2$ Sources: A Contribution to Chemical Energy Conversion, Catalysis Letters 147 (2017) 416–427.

[23] S. Saeidi, N. A. S. Amin, M. R. Rahimpour, Hydrogenation of $CO_2$ to value-added productsA review and potential future developments, Journal of CO2 Utilization 5 (2014) 66–81.

[24] S. G. Jadhav, P. D. Vaidya, B. M. Bhanage, J. B. Joshi, Catalytic carbon dioxide hydrogenation to methanol: A review of recent studies, Chemical Engineering Research and Design 92 (2014) 2557–2567.

[25] I. Ganesh, Conversion of carbon dioxide into methanol a potential liquid fuel: Fundamental challenges and opportunities (a review), Renewable and Sustainable Energy Reviews 31 (2014) 221–257.

[26] K. A. Ali, A. Z. Abdullah, A. R. Mohamed, Recent development in catalytic technologies for methanol synthesis from renewable sources: A critical review, Renewable and Sustainable Energy Reviews 44 (2015) 508–518.

[27] W. Li, H. Wang, X. Jiang, J. Zhu, Z. Liu, X. Guo, C. Song, A short review of recent advances in CO 2 hydrogenation to hydrocarbons over heterogeneous catalysts, RSC Advances 8 (2018) 7651–7669.

[28] D. Sheldon, Methanol Production A Technical History, Johnson Matthey Technology Review 61 (2017) 172–182.

[29] J.-P. Lange, Methanol synthesis: a short review of technology improvements, Catalysis Today 64 (2001) 3–8.

[30] G. Bozzano, F. Manenti, Efficient methanol synthesis: Perspectives, technologies and optimization strategies, Progress in Energy and Combustion Science 56 (2016) 71–105.

[31] V. Palma, E. Meloni, C. Ruocco, M. Martino, A. Ricca, State of the Art of Conventional Reactors for Methanol Production, Methanol (2018) 29–51.

[32] J. J. Meyer, P. Tan, A. Apfelbacher, R. Daschner, A. Hornung, Modeling of a Methanol Synthesis Reactor for Storage of Renewable Energy and Conversion of $CO_2$ - Comparison of Two Kinetic Models, Chemical Engineering and Technology 39 (2016) 233–245.

[33] G. H. Graaf, E. J. Stamhuis, A. Beenackers, Kinetics of low-pressure methanol synthesis, Chemical Engineering Science 43 (1988) 3185–3195.

[34] K. Bussche, G. Froment, A Steady-State Kinetic Model for Methanol Synthesis and the Water Gas Shift Reaction on a Commercial Cu/ZnO/Al2O3Catalyst, Journal of Catalysis 161 (1996) 1–10.

[35] F. Samimi, M. Feilizadeh, M. Ranjbaran, M. Arjmand, M. R. Rahimpour, Phase stability analysis on green methanol synthesis process from $CO_2$ hydrogenation in water cooled, gas cooled and double cooled tubular reactors, Fuel Processing Technology 181 (2018) 375–387.

[36] G. Leonzio, E. Zondervan, P. U. Foscolo, Methanol production by $CO_2$ hydrogenation: Analysis and simulation of reactor performance, International Journal of Hydrogen Energy 44 (2019) 7915–7933.

[37] X. Cui, S. K. Kær, Thermodynamic analysis of steam reforming and oxidative steam reforming of propane and butane for hydrogen production, International Journal of Hydrogen Energy 43 (2018) 13009–13021.

[38] E. L. Fornero, D. L. Chiavassa, A. L. Bonivardi, M. A. Baltanás, $CO_2$ capture via catalytic hydrogenation to methanol: Thermodynamic limit vs. kinetic limit, Catalysis Today 172 (2011) 158–165.

[39] M. J. Bos, D. W. F. Brilman, A novel condensation reactor for efficient $CO_2$ to methanol conversion for storage of renewable electric energy, Chemical Engineering Journal 278 (2015) 527–532.

[40] C. V. Miguel, M. A. Soria, A. Mendes, L. M. Madeira, Direct $CO_2$ hydrogenation to methane or methanol from post-combustion exhaust streams A thermodynamic study, Journal of Natural Gas Science and Engineering 22 (2015) 1–8.

[41] A. Ateka, P. Pérez-Uriarte, M. Gamero, J. Ereña, A. T. Aguayo, J. Bilbao, A comparative thermodynamic study on the $CO_2$ conversion in the synthesis of methanol and of DME, Energy 120 (2017) 796–804.

[42] K. Stangeland, H. Li, Z. Yu, Thermodynamic Analysis of Chemical and Phase Equilibria in $CO_2$ Hydrogenation to Methanol, Dimethyl Ether, and Higher Alcohols, Industrial and Engineering Chemistry Research 57 (2018) 4081–4094.

[43] S. S. Iyer, T. Renganathan, S. Pushpavanam, M. Vasudeva Kumar, N. Kaisare, Generalized thermodynamic analysis of methanol synthesis: Effect of feed composition, Journal of CO2 Utilization 10 (2015) 95–104.

[44] A. G. Dixon, An improved equation for the overall heat transfer coefficient in packed beds, Chemical Engineering and Processing: Process Intensification 35 (1996) 323–331.

[45] B. Koning, Heat and Mass transport in tubular packed bed reactor at reacting and non-reacting conditions, Ph.D. thesis, University of Twente, 2002.

[46] A. G. Dixon, Fixed bed catalytic reactor modelling-the radial heat transfer problem, Canadian Journal of Chemical Engineering 90 (2012) 507–527.

[47] R. H. Perry, D. W. Green, Perrys chemical engineers handbook (eighth ed.), McGraw-Hill, 2008.

[48] X. Cui, S. K. Kær, Two-dimensional thermal analysis of radial heat transfer of monoliths in small-scale steam methane reforming, International Journal of Hydrogen Energy 43 (2018) 11952–11968.

[49] Sandvik, SAF2205, https://www.materials.sandvik/en/materials-center/material-datasheets/tube-and-pipe-seamless/sandvik-saf-2205/, 2019. Accessed July, 2019.

[50] G. H. Graaf, H. Scholtens, E. J. Stamhuis, A. A. C. M. Beenackers, Intra-particle diffusion limitations in low-pressure methanol synthesis, Chemical Engineering Science 45 (1990) 773–783.

[51] B. Lommerts, G. Graaf, A. Beenackers, Mathematical modeling of internal mass transport limitations in methanol synthesis, Chemical Engineering Science 55 (2000) 5589–5598.

[52] Ansys Fluent 19.0, Theory guide, 2018.

[53] L. Chen, Q. Jiang, Z. Song, D. Posarac, Optimization of Methanol Yield from a Lurgi Reactor, Chemical Engineering and Technology 34 (2011) 817–822.

[54] S. Robin, Chemical process: Design and integration, Wiley an Sons, 2005.

*Supporting Information*

# A comparative study on three reactor types for methanol synthesis from syngas and $CO_2$

Xiaoti Cui*, Søren Knudsen Kær

Department of Energy Technology, Aalborg University, 9220 Aalborg, Denmark

*Corresponding author:

Xiaoti Cui

Tel: +45 2667 8192;

E-mail: xcu@et.aau.dk;

# *Appendix A*

## 1. The kinetics for the methanol synthesis process

The reaction kinetics proposed by Bussche and Froment [1] was used to evaluate the reaction rates under different conditions. The reaction rates for the methanol synthesis reaction (reaction (2) in the paper) and reverse water gas shift (RWGS) reaction (reaction (3) in the paper) are expressed by

$$r_{MeOH} = k_d \frac{P_{CO2}P_{H2} - {K_1}^{-1}P_{H2O}P_{MeOH}/P_{H2}^2}{(1 + k_cP_{H2O}/P_{H2} + k_aP_{H2}^{0.5} + k_bP_{H2O})^3} \quad (1)$$

$$r_{RWGS} = k_e \frac{P_{CO2} - K_2P_{H2O}P_{CO}/P_{H2}}{1 + k_cP_{H2O}/P_{H2} + k_aP_{H2}^{0.5} + k_bP_{H2O}} \quad (2)$$

where $r$ is reaction rate (mol/($kg_{cat}$·s)), $k_d$ and $k_e$ are the kinetic factors, $k_a$, $k_b$ and $k_c$ are the adsorption constants, $K_1$ and $K_2$ are the equilibrium constants which can be expressed by [2]

$$K_1 = 10^{-10.592+\frac{3066}{T}} \approx \exp(-24.389 + \frac{7059.726}{T}) \quad (3)$$

$$K_2 = 10^{2.029+\frac{-2073}{T}} \approx \exp(-4.672 + \frac{4773.26}{T}) \quad (4)$$

The parameters for the equations (1) and (2) are shown in Table S1.

Table S1. Parameters for the kinetic equations.

| $k = A \cdot e^{B/RT}$ | A | B |
|---|---|---|
| $k_a$ [$bar^{-0.5}$] | 0.499 | 17197 |
| $k_b$ [$bar^{-1}$] | $6.62\times10^{-11}$ | 124119 |
| $k_c$ [—] | 3453.38 | - |
| $k_d$ [mole/(kg·s·$bar^2$] | 1.07 | 36696 |
| $k_e$ [mole/(kg·s·bar] | $1.22\times10^{10}$ | −94765 |

Based on the above kinetics, the parameters required for Aspen plus are shown in Table S2 where the units of bar and kmol was used for the pressure, and of kmol/($kg_{cat}$·s) was used for reaction rate. Similar parameters based on the unit of Pascal were also mentioned in the literature [3].

Table S2. The input values in Aspen plus for the kinetic equations.

| $k_i = k \cdot exp(-E/RT)$ | $k$ | $E$ |
|---|---|---|
| $k_d$ | 0.00107, kmol/($kg_{cat}$·s·$bar^2$) | −36696, kJ/kmol |
| $k_e$ | $1.22\times10^7$, kmol/($kg_{cat}$·s·bar) | 94765, kJ/kmol |

| $lnK_i = A_i + B_i/T$ | $A_i$ | $B_i$ |
|---|---|---|
| $ln(1/K_1)$ | 24.389 | −7059.726 |
| $lnK_2$ | −4.762 | 4773.16 |
| $lnK_a$ | −0.695149 | 2068.44 |
| $lnK_b$ | -23.438 | 14928.92 |
| $lnK_c$ | 8.14711 | - |

**2. The reaction enthalpy**

The reaction enthalpies $\Delta H_2$ (J/kmol) and $\Delta H_3$ (J/kmol) for reaction (2) and (3) at different temperatures are approximated by the following equations according to the calculations from Aspen Properties.

$$\Delta H_{MeOH} = 3.5895 \times 10^4 T + 4.0047 \times 10^7 \quad (5)$$

$$\Delta H_{RWGS} = 9.177 \times 10^3 T - 4.4325 \times 10^7 \quad (6)$$

3. **Ergun equation**

The pressure drop over the catalyst bed is given by the Ergun equation:

$$\frac{dP}{dz} = -(1.75 + 150\frac{1-\varepsilon}{Re_p})\frac{1-\varepsilon}{\varepsilon^3}\frac{\rho_f u^2}{d_p} \quad (7)$$

## *Appendix B*

Table S3. Simulation results for the adiabatic CTM process with the recycle stream under different pressures

| | Stream S1 | Stream S3 | Stream S4 | Stream S1 | Stream S3 | Stream S4 | Stream S1 | Stream S3 | Stream S4 |
|---|---|---|---|---|---|---|---|---|---|
| P, bar | 30 | 30 | 30 | 50 | 50 | 50 | 80 | 80 | 80 |
| T, ℃ | 100 | 210 | 254.85 | 100 | 210 | 269.49 | 100 | 210 | 284.29 |
| Mole flow rate, kmol/s | 4 | 42.11 | 40.13 | 4 | 32.68 | 30.71 | 4 | 26.77 | 24.80 |
| CO, kmol/s | | 1.1189 | 1.1202 | | 0.5803 | 0.5812 | | 0.3490 | 0.3498 |
| $CO_2$, kmol/s | 1 | 4.1397 | 3.1521 | 1 | 2.6393 | 1.6514 | 1 | 2.0075 | 1.0206 |
| $H_2$, kmol/s | 3 | 36.4601 | 33.5001 | 3 | 29.2761 | 26.3141 | 3 | 24.3134 | 21.3543 |
| $H_2O$, kmol/s | | 0.07437 | 1.0619 | | 0.03628 | 1.0242 | | 0.0204 | 1.0073 |
| $CH_3OH$, kmol/s | | 0.3136 | 1.2998 | | 0.1487 | 1.1357 | | 0.0803 | 1.0664 |
| Mole fraction | | | | | | | | | |
| CO | | 0.02657 | 0.02791 | | 0.01776 | 0.01893 | | 0.01304 | 0.01410 |
| $CO_2$ | 0.25 | 0.09831 | 0.07854 | 0.25 | 0.08076 | 0.05378 | 0.25 | 0.07499 | 0.04116 |
| $H_2$ | 0.75 | 0.86590 | 0.83470 | 0.75 | 0.89582 | 0.85695 | 0.75 | 0.90821 | 0.86112 |
| $H_2O$ | | 0.00177 | 0.02646 | | 0.00111 | 0.03335 | | 0.00076 | 0.04062 |
| $CH_3OH$ | | 0.00745 | 0.03239 | | 0.00455 | 0.03699 | | 0.00300 | 0.04300 |

## *Appendix C*

### 1. The radial Heat transfer in the fixed bed reactor (water-cooled or gas-cooled)

The radial heat transfer between the gas phase in the fixed bed and the boiling water in the shell side can be further described by the heat transfer behavior in the following zones: (1) fixed bed; (2) near-wall region; (3) tube wall and (4) the boiling water outside the tube (for water-cool reactor) or cold gas inside the tube (for gas-cooled reactor). The overall heat transfer coefficient can be expressed by

$$U = \frac{1}{(\frac{1}{U_t} + \frac{b}{k_w} + \frac{1}{h_f})} \tag{8}$$

where $U_t$ is the overall heat transfer coefficient of the fixed bed and near-wall region, $b$ and $k_w$ are the thickness and thermal conductivity of the reactor tube, respectively. $h_f$ is the heat transfer coefficient for the boiling water outside the reactor tube or cold feed inside the reactor tube. For the water-cooled reactor, the heat resistance for the boiling water outside the tube was not considered in this study due to its much higher heat transfer coefficient than other zones [4]. The overall heat transfer coefficient $U_t$ can be evaluated by [5]

$$\frac{1}{U_t} = \frac{1}{h_w} + \frac{R_t}{3k_{e,r}} \frac{Bi + 3}{Bi + 4} \tag{9}$$

where $h_w$ is the wall heat transfer coefficient, $k_{e,r}$ is the effective radial thermal conductivity, $R_t$ is tube radius, $Bi$ is tube Biot number. The calculations of $k_{e,r}$ and $h_w$ are given by the following correlations:

(1) Fixed bed

The heat transfer in the fixed bed was evaluated by the effective radial thermal conductivity $k_{e,r}$ as the following expression [4]:

$$\frac{k_{e,r}}{k_f} = \frac{k_r^0}{k_f} + \frac{Pe_h^0}{Pe_{h,r}^\infty} \tag{10}$$

where $k_r^0$ is effective stagnant thermal conductivity, $k_f$ is thermal conductivity of the gas phase, $Pe_h^0$ is fluid Peclet number for heat transfer and $Pe_{h,r}^\infty$ is Peclet radial heat transfer for fully developed turbulent flow. $k_r^0$ can be calculated by [4]

$$\frac{k_r^0}{k_f} = \left(1 - \sqrt{1-\varepsilon}\right) + \frac{2\sqrt{1-\varepsilon}}{1 - B\kappa^{-1}} \left[ \frac{B(1-\kappa^{-1})}{(1-B\kappa^{-1})^2} \ln\left(\frac{\kappa}{B}\right) - \frac{B-1}{1-B\kappa^{-1}} + \frac{B+1}{2} \right] \tag{11}$$

$$B = C_f \left(\frac{1-\varepsilon}{\varepsilon}\right)^{1.11}; C_f = 1.25\ (sphere), 2.5\ (cylinder) or\ 2.5\left(1 + \frac{d_i}{d_p}\right)(rings) \tag{12}$$

where κ is the ratio of the thermal conductivity of the solid catalyst pellet and the gas fluid $k_p/k_f$, and was approximated by the following equation for aluminum particles [4]:

$$k_p = 0.21 + 0.00015T \tag{13}$$

The fluid Peclet number for heat transfer can in equation (2) is given by

$$\mathrm{Pe}_h^0 = \frac{u\rho_f c_{p,f} d_p^v}{k_f} = RePr \tag{14}$$

where $u_0$ is velocity of the gas phase, $\rho_f$ and $c_{p,f}$ are density and heat capacity of the gas phase, $d_p^v$ is the volume-equivalent particle diameter of the catalyst pellet, for a cylinder pellet with a height $h$ and diameter $d$, the $d_p^v$ can be calculated by

$$d_p^v = d(\frac{3h}{2d})^{\frac{1}{3}} \tag{15}$$

The $Pe_{h,r}^{\infty}$ value in equation (2) can be evaluated by [4, 6]

$$Pe_{h,r}^{\infty} = 8\left[2 - \left(1 - \frac{2}{N}\right)^2\right] \tag{16}$$

where $N$ is the ratio of the tube diameter and volume-equivalent diameter, $N=D_t/d_p^v$.

(2) Near-wall region

The effect of the tube wall on the radial heat transfer is considered by the wall Nusselt number $Nu_w$ which is given by the expressions [6]:

$$Nu_w = Nu_{w0} + (1/Nu_W^* + 1/Nu_m)^{-1} \tag{17}$$

$$Nu_{w0} = (1.3 + \frac{5}{N})(\frac{k_r^0}{k_f}) \tag{18}$$

$$Nu_w^* = 0.3Pr^{1/3}Re^{0.75} \tag{19}$$

$$Nu_m = 0.054PrRe \tag{20}$$

(3) Cold feed

Different from the large heat transfer coefficient $h_f$ for the boiling water in a water-cooled reactor, the $h_f$ value for the cold feed in the reactor tube of a gas-cooled reactor could be much lower and should be considered. In this study, the heat transfer coefficient is approximated by the Dittus-Boelter equation [7]:

$$Nu_f = 0.243Pr^{0.4}Re^{0.8} \tag{21}$$

**2. Parameters and results for the modeling of radial heat transfer (water-cooled reactor)**

Table S4. Parameters and results for the radial heat transfer calculations in Section 3.2.

| Cross-sections in Fig.6 | A | B | C | D | E | F |
|---|---|---|---|---|---|---|
| Gas composition at the hot-spots, mole fraction | | | | | | |
| CO | 0.0271 | 0.0398 | 0.0565 | 0.0221 | 0.0318 | 0.0472 |
| $CO_2$ | 0.0593 | 0.0456 | 0.0353 | 0.0488 | 0.0374 | 0.0292 |
| $H_2$ | 0.8609 | 0.8685 | 0.8650 | 0.8743 | 0.8794 | 0.8736 |
| $H_2O$ | 0.0267 | 0.0172 | 0.0108 | 0.0285 | 0.0193 | 0.0123 |
| MeOH | 0.0260 | 0.0289 | 0.0324 | 0.0263 | 0.0321 | 0.0378 |
| Effective thermal conductivity and heat transfer coefficient | | | | | | |
| $k_{r,e}$,* W/(m·K) | 6.2 | 6.2 | 6.1 | 6.4 | 6.2 | 6.4 |
| $h_w$,* W/($m^2$·K) | 472.7 | 473.0 | 468.2 | 483.5 | 475.9 | 485.5 |
| $U$, W/($m^2$·K) | 321.7 | 321.5 | 318.1 | 341.5 | 323.5 | 330.2 |
| Average temperature calculated by CFD ($T_1$) and pseudo-homogeneous model ($T_2$), ℃ | | | | | | |
| $T_1$, ℃ | 256 | 263 | 269 | 257 | 267 | 278 |
| $T_2$, ℃ | 256 | 263 | 271 | 257 | 268 | 280 |

*: the thermal conductivity and wall heat transfer coefficient were calculated according to the average physical properties at the inlet and outlet of the reactor.

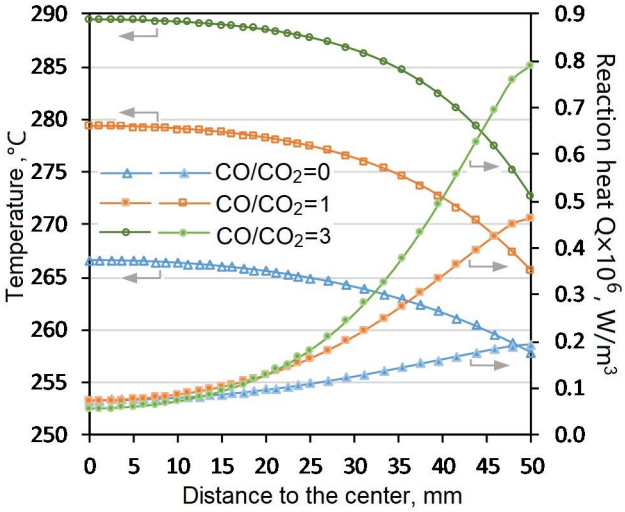


Figure S1. Radial temperature profile and reaction heat at the hot-spots for the equivalent tube with different $CO/CO_2$ ratios for feed stream S1; P= 50 bar and tube radius of 50 mm.

3**. CFD simulations for the radial heat transfer (gas-cooled reactor)**

The catalyst bed in the shell side of the gas-cooled reactor was approximated by a multi-tube structure with an equivalent tube diameter of 58–60 mm. CFD simulations were conducted to roughly evaluated the local hot-spot temperature in the "tube".

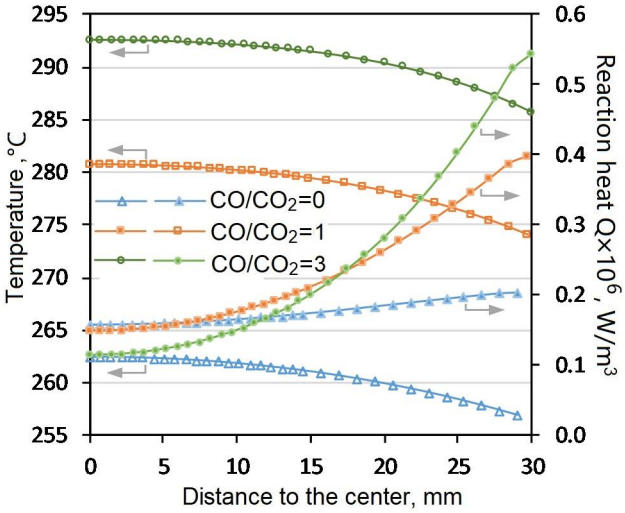


Figure S2. "Radial" temperature profile and reaction heat at the hot-spots for the equivalent tube with different $CO/CO_2$ ratios for feed stream S1; P= 50 bar.

## *Appendix D*

### 1. The diffusion coefficients

The effective diffusivity $D_{i,eff,S}$ based on the Maxwell-Stefan equations is expressed by [8]

$$\frac{1}{D_{i,eff,S}} = \sum_{\substack{j=1 \\ j\neq i}}^{n} \frac{Y_j}{D_{ij}} \left(1 - \frac{Y_i N_j}{Y_j N_i}\right) \tag{22}$$

where $N$ and $Y$ are the mass flux and mass fraction, respectively; $D_{ij}$ is the Fick's law binary diffusion coefficient, which is calculated by the Chapman-Enskog equation [7]. In this study, the $D_{i,eff,S}$ value of was obtained from the full multicomponent diffusion modeling in the Ansys Fluent software.

The Knudsen diffusion coefficient for the $i^{th}$ species is calculated by [7]

$$D_{i,K} = 97 r_p \sqrt{T/M_i} \tag{23}$$

where $r_p$ is the mean pore radius (m) in the catalyst pellet, and a value of 10 nm [9] was employed in this study for the methanol synthesis catalyst.

## *Appendix E*

Table S5. The key design parameters and performance indicators for the three reactors

| | Adiabatic | Water-cooled | Gas-cooled |
|---|---|---|---|
| Stream S1 | | | |
| $H_2$, kmol/h | 48 | 48 | 48 |
| $CO_2$, , kmol/h | 16 | 16 | 16 |
| $T_{in}$, ℃ | 215 | 210 | 235 |
| Operating pressure, bar | 80 | 80 | 80 |
| Tube I.D., mm | | 40 | 25 |
| Tube O.D., mm | | 44 | 29 |
| Tube number | | 308 | 290 |
| Reactor, I.D. m | 0.702 | 1.34 | 0.859 |
| Reactor length, m | 3 | 3 | 3 |
| Catalyst volume, $m^3$ | 1.16 | 1.16 | 1.16 |
| GHSV, $h^{-1}$ | 13282 | 10328 | 10311 |
| *Heat transfer coefficient,* W/($m^2$·K) | | 326.7 | 79.8 |
| $T_{max}$, ℃ | 259.3 | 257.4 | 261.0 |
| Recycle ratio | 10 | 7.61 | 7.60 |
| Single-pass methanol yield | 22.4% | 31.7% | 31.4% |

## *Appendix F*

The capital cost for the CTM process with the three reactors were evaluated by [10]

$$C_c = C_B(Q_c/Q_B)^M f_M f_P f_T \quad (24)$$

where $C_B$ and $Q_B$ are the base cost and base capacity, respectively, $Q_C$ is the design component capacity, M is the cost exponent, $f_M$, $f_P$ and $f_T$ are the material of construction capital cost factor, pressure correction factor and temperature correction factor, respectively. The cooler in Figure 1(a) in the paper has been replaced by four heat exchangers (shown in Figure S3) considering a possible case of heat integration for the CTM process. A second flash tank (Separator 2) has also been added with a pressure of 3bar and temperature of 30℃.

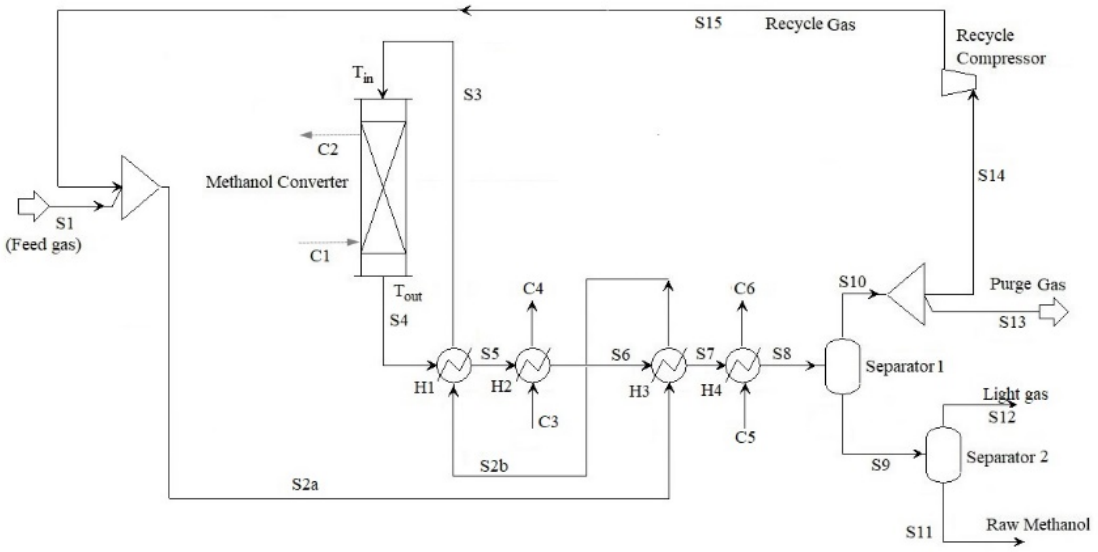


Figure S3. Scheme of the CTM process with heat integration.

As shown in Figure S3, the hot stream S4 from the outlet of the reactor was cooled when flowing through the four heat exchangers from H1 to H4. The temperature setting for the heat exchangers are shown in Table S6. Temperature of stream S6 was adjusted between 120℃ and 130℃ to fulfill the requirement of a minimum temperature approach of 15℃. The stream C3 is hot water with the temperature close to that of the reboiler for the methanol distillation column, where H2 can be the reboiler. The heat exchange for S7 was simplified by H4, where C5 is cooling water. There could also be air cooling involved for this part. Notably, there could be several other different heat integration cases for a real methanol plant. The heat transfer areas for the heat exchangers were approximated by the shortcut method in Aspen Plus.

The pressure drops for H1 to H4 were not calculated, while the total pressure drop from S3 to S14 was assumed to be 2 bar, and the pressure increase by the recycle compressor is set to be 3 bar with a compressor efficiency of 0.55. The total pressure drop from S15 to S3 was assumed to be 1 bar. The volume of the steam drum for the water-cooled reactor was evaluated by the evaporation volume of boiling water for 15 minutes. The volumes of the flash tanks (Separator 1 and 2) were estimated by the storage of stream S9 and S11 for 5 minutes, respectively.

Table S6. The design parameters for the heat exchangers

| | S5 | S6 | S8 | C3 | C5 | C6 |
|---|---|---|---|---|---|---|
| Temperature, ℃ | 160 | 120−130 | 40 | 99 | 25 | 70 |
| Flow rate, kmol/h | | | | 20 | 470−520 | |

The reactor weight, heat exchanger area, compression power and separator volume were calculated by the simulations using Aspen Plus. The capital cost for the components of the reactors, heat exchangers, compressor and flash tanks were calculated by equation (24), where the relevant parameter values are shown in Table S7, which have been adjusted according to the values in the literature [10].

Table S7. The parameter values for the capital cost calculation.

| | $C_B$($) | $M$ | $f_M$ | $f_M$ | $f_M$ |
|---|---|---|---|---|---|
| Reactor | 98400 | 0.82 | 1.52 | 1.5 | 1.45 |
| Heat exchanger | 32800 | 0.68 | 2.6 | 1.5 | 1.225 |
| Compressor | 98400 | 0.46 | 1 | 1.5 | 1.15 |
| Separator (and steam drum) | 3280 | 0.57 | 1 | 1.25 | 1 |

**Nomenclature**

| | | |
|---|---|---|
| $b$ | m | Wall thickness of reactor tube |
| $Bi$ | (-) | Tube Bilot number, $h_w R_t/k_{e,r}$ |
| $C_p$ | J $kg^{-1}K^{-1}$ | Heat capacity |
| $d$ | m | Diameter of cylinder pellet |
| $d_p^v$ | m | Diameter of sphere with equal volume |
| $D$ | m or $m^2/s$ | Diameter of reactor tube; diffusion coefficient |
| $h$ | m | Height of cylinder pellet |
| $h_f$ | W $m^{-2}K^{-1}$ | Heat transfer coefficient between reactor wall and boiling water or cold feed |
| $h_w$ | W $m^{-2}K^{-1}$ | Wall heat transfer coefficient |
| $k$ | W/m·K | Thermal conductivity, parameters in reaction rate equations |
| $k_{r,e}$ | W/m·K | Effective radial thermal conductivity |
| $M$ | kg/kmol | Molecular weight |
| $N$ | (-) or kg $m^{-2}s^{-1}$ | Aspect ratio; mass flux |
| $Nu_f$ | (-) | Nusselt number in the reactor tube with cold feed ($h_f D/k_f$) |
| $Nu_w$ | (-) | Wall Nusselt number ($h_w d_p^v/k_f$) |
| $Nu_{w0}$ | (-) | Wall Nusselt number at zero flow rate ($h_{w0} d_p^v/k_f$) |
| $Nu_W^*$ | (-) | Wall film Nusselt number ($h_W^* d_p^v/k_f$) |
| $Nu_m$ | (-) | Fluid mechanical Nusselt number ($h_{wm} d_p^v/k_f$) |
| $P$ | Pa | Pressure |
| $Pe_h^0$ | (-) | Fluid Peclet number for heat transfer ($u\rho_f c_{p,f} d_p^v/k_f$) |
| $Pe_{h,r}^\infty$ | (-) | Peclet radial heat transfer for fully developed turbulent flow |
| $Pr$ | (-) | Prandtl number ($\mu_f c_{p,f}/k_f$) |
| $r_p$ | m | The mean pore radius |
| $R_t$ | m | Radius of reactor tube |
| $Re$ | (-) | Reynolds number ($u\rho_f d_p^v/\mu_f$) |
| $T$ | K | Temperature |
| $u$ | m/s | Superficial gas velocity |
| $U_t$ | W $m^{-2}K^{-1}$ | Overall heat transfer coefficient of the fixed bed and near-wall region |
| $U$ | W $m^{-2}K^{-1}$ | Overall heat transfer coefficient between the gas phase and boiling water |
| $Y$ | (-) | Mass fraction |

*Greek letters*

| | | |
|---|---|---|
| $\varepsilon$ | (-) | Porosity of catalyst bed |
| $\kappa$ | (-) | Ratio of thermal conductivity of solid and fluid |
| $\mu_f$ | kg/m s | Gas viscosity |
| $\rho_f$ | $kg/m^3$ | Gas density |

*Subscripts*

| | |
|---|---|
| *0* | Stagnant |
| *e* | Effective |
| *f* | Gas phase |
| *h* | Heat transfer |

| | |
|---|---|
| *p* | Pellet |
| *r* | Radial |
| *t* | Tube |
| *w* | Wall |

***Reference***

[1] K. Bussche, G. Froment, A steady-state kinetic model for methanol synthesis and the water gas shift reaction on a commercial $Cu/ZnO/Al_2O_3$ catalyst. J. Cata. 161 (1996) 1–10.

[2] G. H. Graaf, P. J. J. M. Sijtsema, E. J. Stamhuis and G. E. H. Joosten. Chemical equilibria in methanol synthesis. Chem. Eng. Sci. 41(1986) 2883–2890.

[3] Leonie E. Lücking. Methanol Production from Syngas Process modelling and design utilising biomass gasification and integrating hydrogen supply, Master Thesis (2017), Delft University of Technology.

[4] B. Koning. Heat and Mass transport in tubular packed bed reactor at reacting and non-reacting conditions, PhD Thesis (2002), University of Twente.

[5] A. G. Dixon, An improved equation for the overall heat transfer coefficient in packed beds, Chemical Engineering and Processing 35 (1996) 323–331.

[6] A. G. Dixon. Fixed Bed Catalytic Reactor Modelling—the Radial Heat Transfer Problem. Can. J. Chem. Eng. 90 (3) (2012) 507–527.

[7] R.H. Perry, D.W. Green. Perry's Chemical Engineers' Handbook (eighth ed.), McGraw-Hill, New York (2008).

[8] R. Taylor, R. Krishna. Multicomponent Mass Transfer, Wiley, New York (1993).

[9] G. H. Graaf, H. Scholtens, E. J. Stamhuis, A. A. C. M. Beenackers, Intra-particle diffusion limitations in low-pressure methanol synthesis, Chemical Engineering Science 45 (1990) 773–783.

[10] R. Smith. Chemical process: design and integration. Wiley and Sons, 2005.